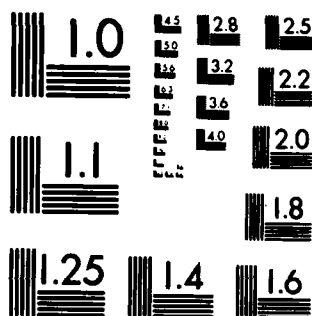


UNCLASSIFIED

F/G 9/1

NL

END
DATE
FILMED
4 1964
DTIC

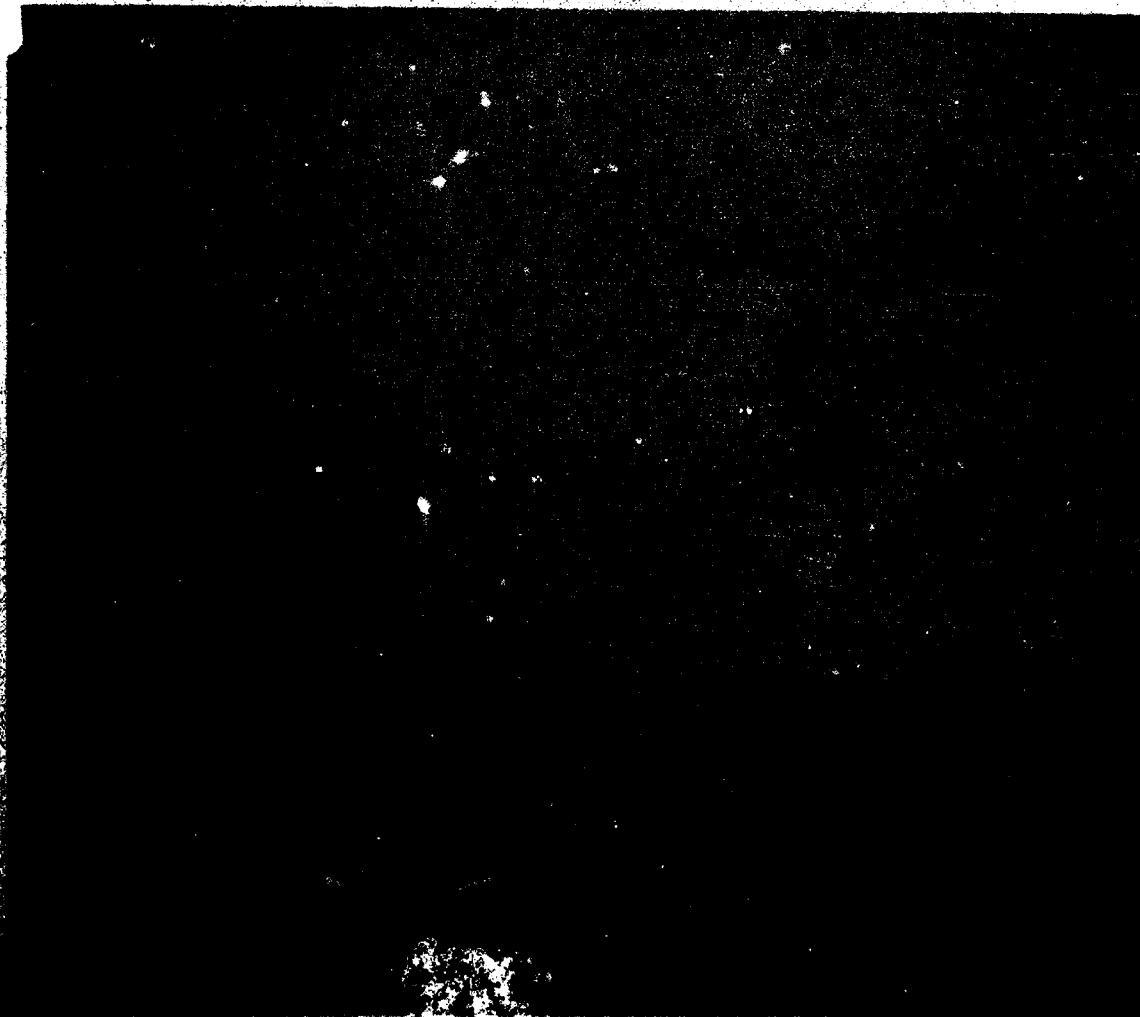


MICROCOPY RESOLUTION TEST CHART
NATIONAL BUREAU OF STANDARDS-1963-A

ADA 124363

COORDINATED SCIENCE LABORATORY

**INVESTIGATION OF METAL TO
DIELECTRIC WAVEGUIDE TRANSITION
AND THE COUPLING CHARACTERISTICS
OF DIELECTRIC WAVEGUIDES
OF RECTANGULAR CROSS SECTION**



REPORT DOCUMENTATION PAGE		READ INSTRUCTIONS BEFORE COMPLETING FORM
1. REPORT NUMBER	2. GOVT ACCESSION NO. AD A724 363	3. RECIPIENT'S CATALOG NUMBER
4. TITLE (and Subtitle) INVESTIGATION OF METAL TO DIELECTRIC WAVEGUIDE TRANSITION AND THE COUPLING CHARACTERISTICS OF DIELECTRIC WAVEGUIDES OF RECTANGULAR CROSS-SECTION		5. TYPE OF REPORT & PERIOD COVERED Technical Panel
7. AUTHOR(s) Trang Nha Trinh		6. PERFORMING ORG. REPORT NUMBER R-899; UIU ENG-80-2230
9. PERFORMING ORGANIZATION NAME AND ADDRESS Coordinated Science Laboratory University of Illinois Urbana, Illinois 61801		8. CONTRACT OR GRANT NUMBER(s) U.S. Navy N00014-79-C-0424
11. CONTROLLING OFFICE NAME AND ADDRESS Joint Services Electronics Program		10. PROGRAM ELEMENT, PROJECT, TASK AREA & WORK UNIT NUMBERS
14. MONITORING AGENCY NAME & ADDRESS (if different from Controlling Office)		12. REPORT DATE October, 1980
		13. NUMBER OF PAGES 49
		15. SECURITY CLASS. (of this report) UNCLASSIFIED
		15a. DECLASSIFICATION/DOWNGRADING SCHEDULE
16. DISTRIBUTION STATEMENT (of this Report) Approved for public release; distribution unlimited		
17. DISTRIBUTION STATEMENT (of the abstract entered in Block 20, if different from Report)		
18. SUPPLEMENTARY NOTES		
19. KEY WORDS (Continue on reverse side if necessary and identify by block number) Metal to dielectric waveguide transition Coupling characteristics of dielectric waveguides		
20. ABSTRACT (Continue on reverse side if necessary and identify by block number) The development of an efficient low-loss transition from a conventional metal waveguide to a planar dielectric guide of rectangular cross-section is presented. Such a transition finds important applications in millimeter-wave integrated circuits. We also present an approximate but accurate analytical method based on experimental results for predicting the coupling characteristics of both symmetrical and nonsymmetrical dielectric couplers of rectangular cross-section.		

SECURITY CLASSIFICATION OF THIS PAGE(When Data Entered)

SECURITY CLASSIFICATION OF THIS PAGE(When Data Entered)

UILLU-ENG 80-2230

INVESTIGATION OF METAL TO DIELECTRIC WAVEGUIDE
TRANSITION AND THE COUPLING CHARACTERISTICS OF
DIELECTRIC WAVEGUIDES OF RECTANGULAR CROSS-SECTION

by

Trang Nha Trinh

This work was supported in part by the Joint Services Electronics
Program (U.S. Army, U.S. Navy and U.S. Air Force) under Contract U.S. Navy
N00014-79-C-0424.

Reproduction in whole or in part is permitted for any purpose
of the United States Government.

Approved for public release. Distribution unlimited.

DTIC
COPY
INSPECTED

Accession For	
DTIC	DTIC
DTIC	DTIC
Unannounced Justification	
By	
Distribution/	
Availability Codes	
Dist	Avail and/or Special
A	

INVESTIGATION OF METAL TO DIELECTRIC WAVEGUIDE
TRANSITION AND THE COUPLING CHARACTERISTICS
OF DIELECTRIC WAVEGUIDES OF RECTANGULAR CROSS-SECTION

BY

TRANG NHA TRINH

B.S., Wilkes College, 1978

THESIS

Submitted in partial fulfillment of the requirements
for the degree of Master of Science in Electrical Engineering
in the Graduate College of the
University of Illinois at Urbana-Champaign, 1980

Thesis Advisor: Professor Raj Mittra

Urbana, Illinois

The development of an efficient low-loss transition from a conventional metal waveguide to a planar dielectric guide of rectangular cross-section is presented. Such a transition finds important applications in millimeter-wave integrated circuits. We also present an approximate but accurate analytical method based on experimental results for predicting the coupling characteristics of both symmetrical and nonsymmetrical dielectric couplers of rectangular cross-section.

The development of an efficient low-loss transition from a conventional metal waveguide to a planar dielectric guide of rectangular cross-section is presented. Such a transition finds important applications in millimeter-wave integrated circuits. We also present an approximate but accurate analytical method based on experimental results for predicting the coupling characteristics of both symmetrical and nonsymmetrical dielectric couplers of rectangular cross-section.

TABLE OF CONTENTS

CHAPTER	Page
I. INTRODUCTION	1
II. METAL TO DIELECTRIC WAVEGUIDE TRANSITION	3
A. Tapered Dielectric Waveguide Section	3
B. Flared Metal Horn	6
C. Loss Characteristics	8
C.1. Return Loss	8
C.2. Insertion Loss	8
D. Final Metal Horn Transition Configuration	12
E. Applications	12
III. COUPLING CHARACTERISTICS OF DIELECTRIC WAVEGUIDE OF RECTANGULAR CROSS-SECTION	19
A. Simple Distributed Directional Couplers	19
B. Analyses of Practical Coupling Structures	24
B.1. Nonuniform Spacing Symmetric Couplers	24
B.2. Nonsymmetric Couplers	26
B.3. Coupling Structure Incorporating a Straight Coupling Section with Two Nonsymmetric Arms	31
C. Experimental Verification	36
IV. CONCLUSIONS	41
V. APPENDICES	42
Appendix A: Generalized Effective Dielectric Constant Method	42
Appendix B: Determination of Scattering Coefficients	46
VI. LIST OF REFERENCES	48

LIST OF FIGURES

Figure	Page
1. Improved Transition Mechanism	4
2. Dielectric Taper Section	5
3. Flared Metal Horn	7
4. Return Loss vs. Frequency	9
5. Return Loss vs. Frequency	10
6. Insertion Loss of the Dielectric Waveguide	11
7. Total Insertion Loss	13
8. Dimensions of the Designed Horn	14
9. Comparison of Radiation Patterns in the H-plane for a Dielectric Antenna Using Two Types of Transitions	16
10. Comparison of Radiation Patterns in the H-plane for a Dielectric Antenna Using Two Types of Transitions.	17
11. Comparison of Radiation Patterns of the Metal Horn and the Short Dielectric Antenna Using the Same Metal Horn as Transition	18
12. Typical Millimeter-wave Integrated Circuit	20
13. Cross-Sectional View of the Coupled Structure	21
14. Simple Distributed Directional Coupler	23
15. Nonuniform Spacing Symmetric Coupler	25
16. Scattering Coefficients of a Symmetric Coupler vs. Guide Spacing d_0 at $f = 8.5$ GHz	27
17. Scattering Coefficients of a Symmetric Coupler vs. Guide Spacing d_0 at $f = 9.5$ GHz	28
18. Nonsymmetric Coupler	29

19. Scattering Coefficients of a Nonsymmetric Coupler vs. Guide Spacing d_0 at $f = 8.5$ GHz.....	33
20. Scattering Coefficients of a Nonsymmetric Coupler vs. Guide Spacing d_0 at $f = 9.5$ GHz.....	34
21. Coupling Structure Incorporating a Straight Section and Curved Connecting Arms.....	35
22. Scattering Coefficients of the Coupler Shown in Fig. 21 for $f = 8.5$ GHz.....	37
23. Scattering Coefficients of the Coupler Shown in Fig. 21 for $f = 9.5$ GHz.....	38

LIST OF TABLES

Table	Page
1. Typical Values of the Correction Factor ν for Nonsymmetric Couplers.....	32

I. INTRODUCTION

As frequency is extended to the millimeter-wave range, the integrated circuits using the low-loss dielectric waveguide and image guide as guiding media become very popular. But at current technology, most of the power sources are active devices which are implanted in a metal waveguide. Thus, in order to efficiently transfer the energy from the propagating modes in the metal waveguide to the dielectric waveguide, or vice versa, a well-designed transition is essential. The metal-to-dielectric waveguide transition can also be effectively employed in a millimeter wave integrated circuit to expand the basic circuit configuration without further degrading the performance of the circuit.

An efficient, practical transition must be small, easy-to-fabricate and low loss. The combination of these constraints presents a great challenge to the designers. At present, however, there is little information available in the literature on the design and performance of such a transition.

If the excessive radiation caused by the mismatch at the feed ends can be reduced by using an efficient transition, it is possible to study the coupling characteristics of the opened-structure dielectric components without any interference from strayed radiation. The investigation of the coupling characteristics of the dielectric components is extremely important since, with the increasing use of the dielectric materials as opened-structure guiding media, the interactions among these components become unavoidable.

The coupling characteristics of the dielectric waveguides have been studied by several authors [1], [2], [3]. More recently, Itanami [4] and Anderson [5] have presented approximate calculations for the coupling

between two symmetrically curved dielectric waveguides. Solbach [6] has computed the coupling between two straight dielectric waveguide sections which have symmetric curved ends. All of the coupling structures mentioned above are symmetrical in nature. In this investigation, the techniques for calculating the scattering coefficients of nonsymmetric structures are discussed.

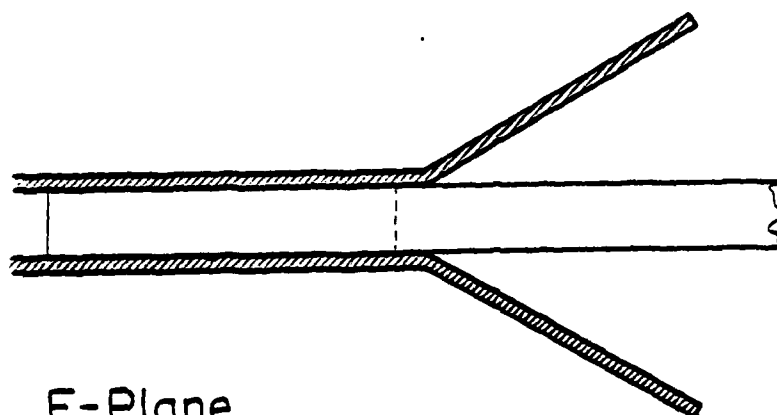
II. METAL-TO-DIELECTRIC WAVEGUIDE TRANSITION

The simplest and still widely used metal-to-dielectric transition with millimeter-wave applications is a straight dielectric waveguide, tapered in both the E and H planes, and inserted into a truncated conventional metal waveguide. Because of the abrupt discontinuity between the metal and the dielectric waveguide, a large amount of energy is converted to radiation. The launching efficiency is degraded due to this radiation loss.

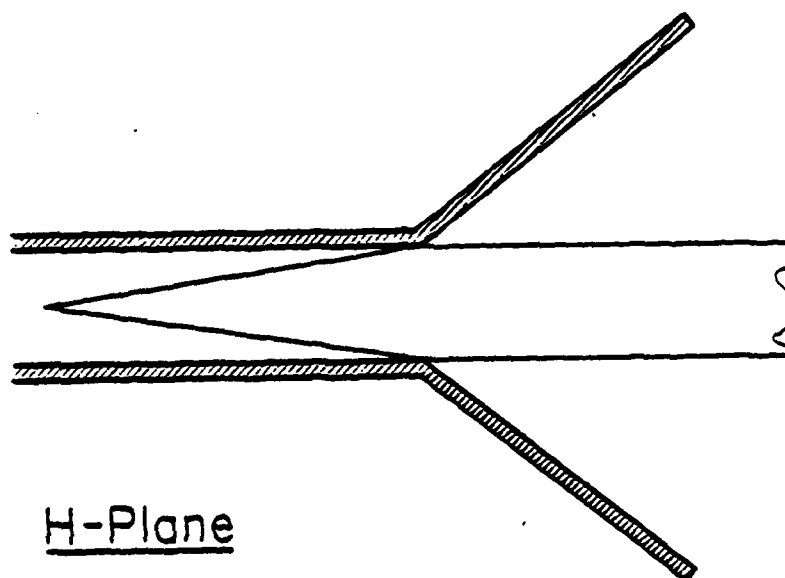
To improve this launching mechanism, several transition configurations were investigated. After a large number of initial experiments, the most practical and efficient configuration was narrowed down to the dielectric tapered section fed by a flared metal horn, which is shown in Figure 1. The dielectric waveguide should be slightly smaller than the inner dimensions of the metal waveguide section. A detailed discussion is described next.

A. Tapered Dielectric Waveguide Section

As a first step, two tapered dielectric waveguide sections were constructed, one of which was tapered both in the E- and H-planes and the other in the H-plane only. The dielectric material used was Teflon with $\epsilon_r = 2.057$ and $\tan\delta = 6.0 \times 10^{-4}$. A sketch of the tapered dielectric waveguide is shown in Figure 2. The solid lines correspond to a taper in the H-plane only, whereas the dotted lines show the taper in both planes. A study of these two tapered sections revealed that for taper lengths on the order of $4 \lambda_g$ or greater the two configurations performed essentially identically. Hence, for the sake of simplicity, in the future experiments, the length of the tapered section was chosen



E-Plane



H-Plane

HP-246

Figure 1. Improved Transition Mechanism

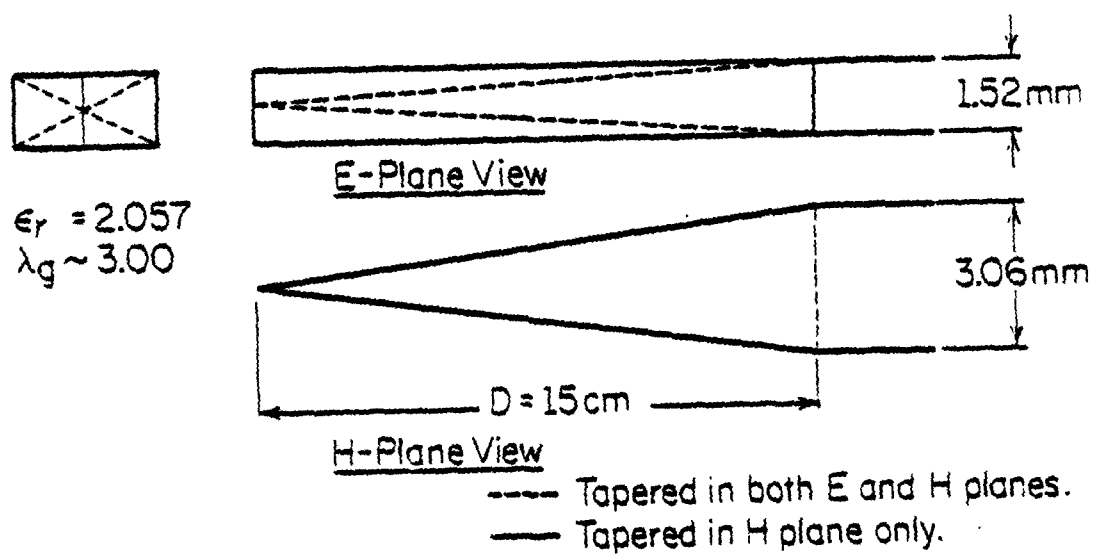


Figure 2. Dielectric Taper Section

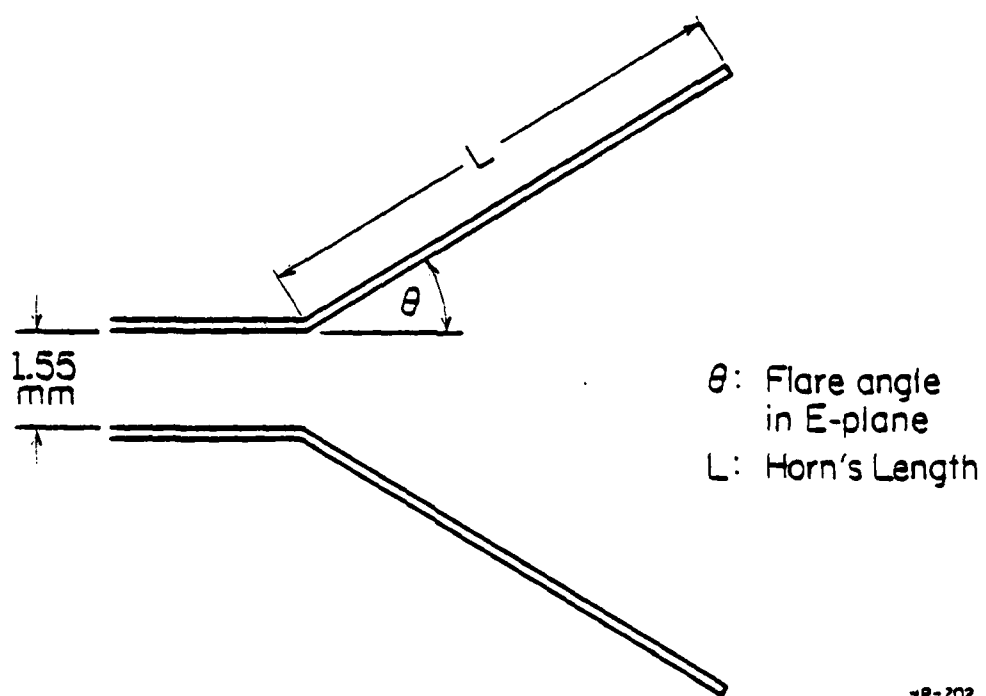
to be about $5\lambda_g$, and the guide was tapered only in the H-plane. The single plane dielectric taper greatly simplified the fabrication of the transition region of the dielectric waveguide.

B. Flared Metal Horn

In order to keep the length of the metal horn as small as possible, the horn length L was chosen to be less than $2\lambda_0$. Thus, the principal design parameter of the horn that needed investigating is its flare angle θ (see Figure 3).

Typically, for the type of dielectric waveguide being considered here, a large percentage of the power in the propagating modes is carried by the medium external to the guide. For a relatively large aspect ratio of the cross section of the guide, the energy is principally concentrated above and below the guide. Consequently, the flare angle in the E-plane has a dominant effect on the behaviour of the transition. Experimental studies confirm that only the flare angle in the E-plane had a significant effect on the performance of the transition. For this reason, the horn angle in the H-plane can be chosen almost arbitrarily, and the angle of the E-plane taper was used as the variable parameter.

It is important to realize that the aspect ratio of the dielectric waveguide has been deliberately chosen to be large, which is the case for many practical applications, in order to minimize the field intensities in the H-plane outside of the dielectric waveguide. By doing so, most of the energy is concentrated only above and below the dielectric guide. The investigation is therefore simpler due to the fact that only the flare angle in the E-plane needed investigating.



4P-202

Figure 3. Flared Metal Horn

C. Loss Characteristics

C.1. Return Loss

For a system consisting of two transitions and a dielectric waveguide section of roughly $40 \lambda_0$, the return loss was measured as a function of frequency for various E-plane tapered angle θ . The result is shown in Figure 4. When the flare angle θ was varied from 22-39 degrees for a fixed horn length, the return loss remained less than 16 dB (VSWR < 1.4) throughout the frequency range. For the sake of clarity, only the return loss of the systems with the flare angles $\theta = 22, 30$ and 39 degrees were plotted, although many other angles were studied.

In order to illustrate the significant improvement achieved by a proper choice of the flare-angle range, the results for the two extreme cases, viz., $\theta = 90$ and $\theta = 0$ degrees which are still extensively employed in many MMWICs, are also presented (see Figure 5). At many instances, the return loss for these cases is less than 6 dB (VSWR > 3.0).

C.2. Insertion Loss

The total insertion loss comprises the dielectric loss of the waveguide and the loss due to the transitions. In order to isolate the dielectric loss, the system was measured for two different lengths of guide, and the loss figure for the shorter length was subtracted from that of the longer one. This procedure eliminates the loss contribution due to the two metal transitions, thus yielding the loss figure for the dielectric waveguide alone [4], [7]. Figure 6 shows the computed and experimental results for a 3.0 mm wide and 1.5 mm high dielectric waveguide made of Teflon with $\epsilon_r = 2.057$ and $\tan \delta = 6.0 \times 10^{-4}$.

$\theta = 30^\circ$ —
 $\theta = 39^\circ$
 $\theta = 22^\circ$ ---

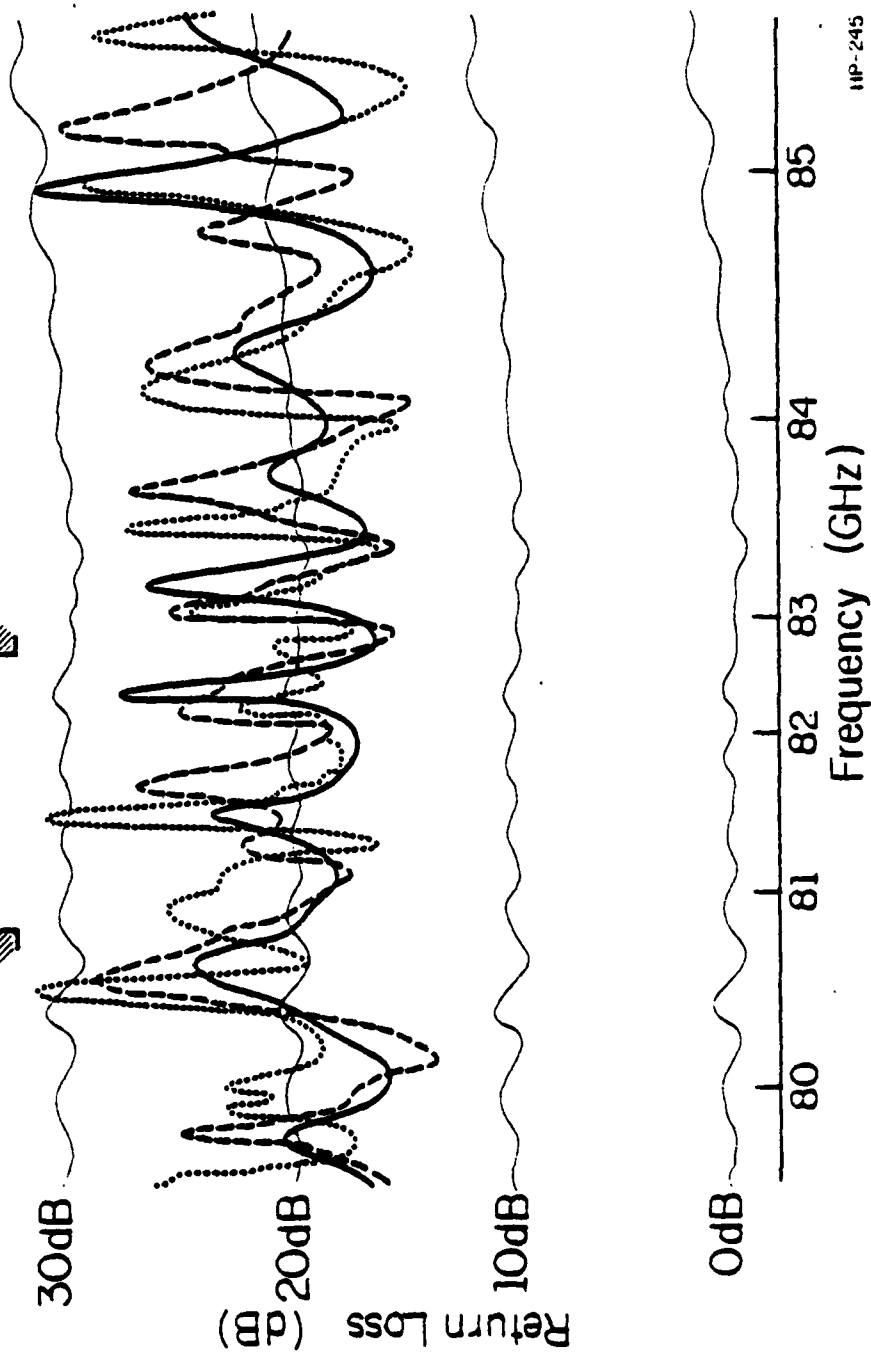
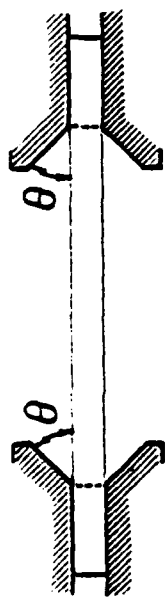


Figure 4. Return loss vs. Frequency

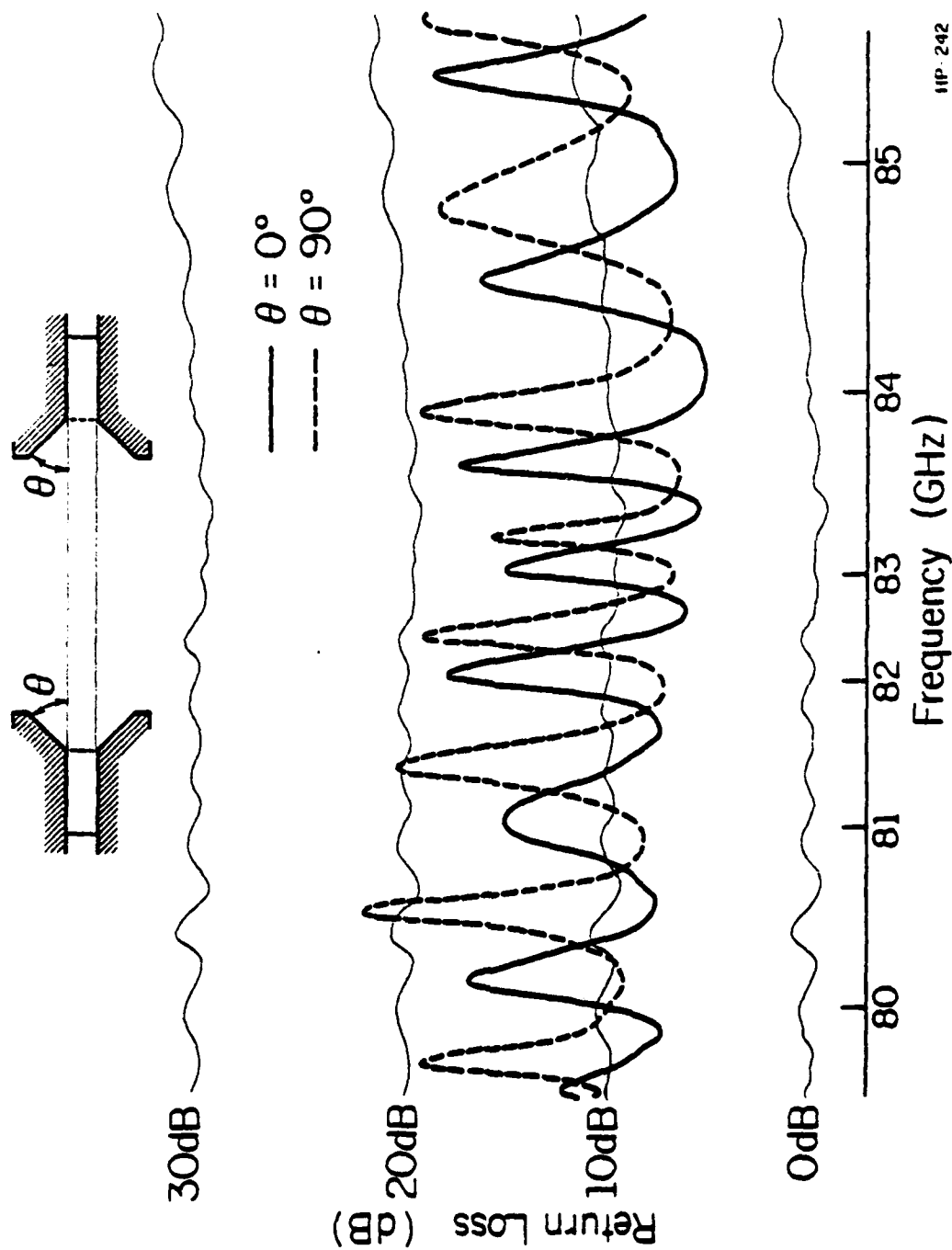


Figure 5. Return Loss vs. Frequency

HP-242

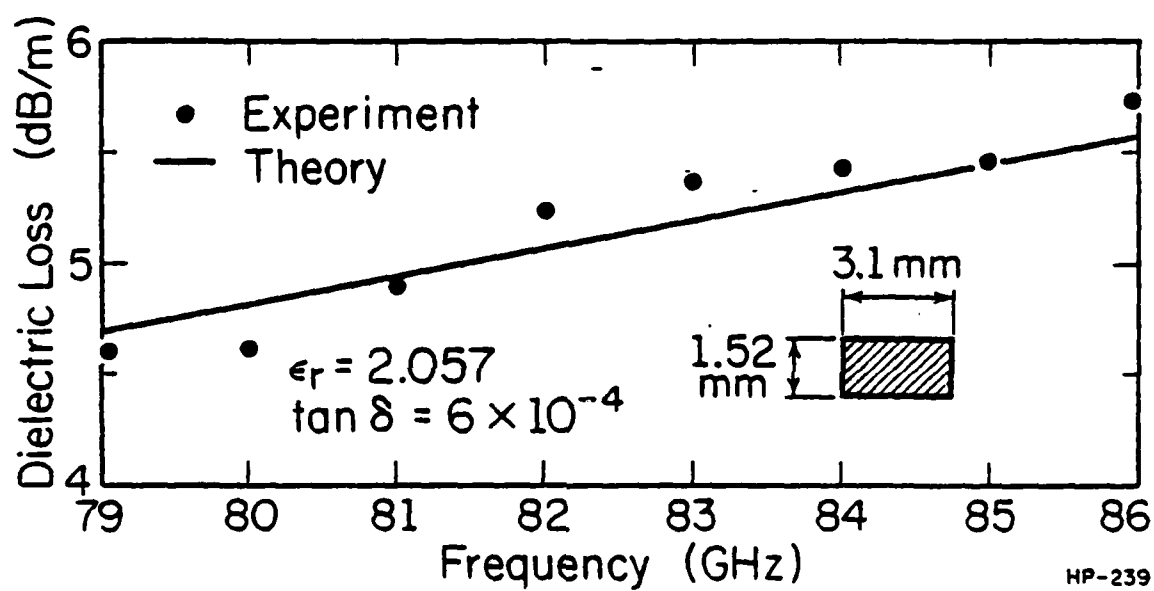


Figure 6. Insertion Loss of the Dielectric Waveguide

The total insertion loss for a dielectric waveguide section of $40 \lambda_0$ long and two transitions is shown in Figure 7 as a function of frequency for various horn angles θ . The loss due to two transitions alone was obtained by subtracting the loss of the dielectric waveguide section, which has been described in the previous paragraph, from this total loss. Figure 7 shows the loss due to the mismatch at the transitions to be on the average of 0.5 dB, and always less than 1 dB throughout a broad frequency range from 79 to 86 GHz. This loss figure is believed to be satisfactory by any standard.

As a comparison, the very high insertion losses of the transitions with the conventional flare angles, i.e., $\theta = 0$ or 90 degrees, are also presented.

D. Final Metal Horn Transition Configuration

On the basis of this study, the flare angle θ in the E-plane was henceforth fixed at 31 degrees. Using the ratio of E- and H-plane dimensions of an ordinary horn as a guide, the corresponding flare angle in the H-plane was chosen to be 35 degrees although, for the given guide dimensions, the flare angle in the H-plane can almost be chosen arbitrarily. The final design of the horn obtained in this manner is shown in Figure 8.

E. Applications

With the radiation losses reduced to a minimum figure, a well-designed metal-to-dielectric transition described above finds many useful applications in a millimeter-wave integrated circuit. By employing these transitions, a basic circuit configuration can be expanded considerably

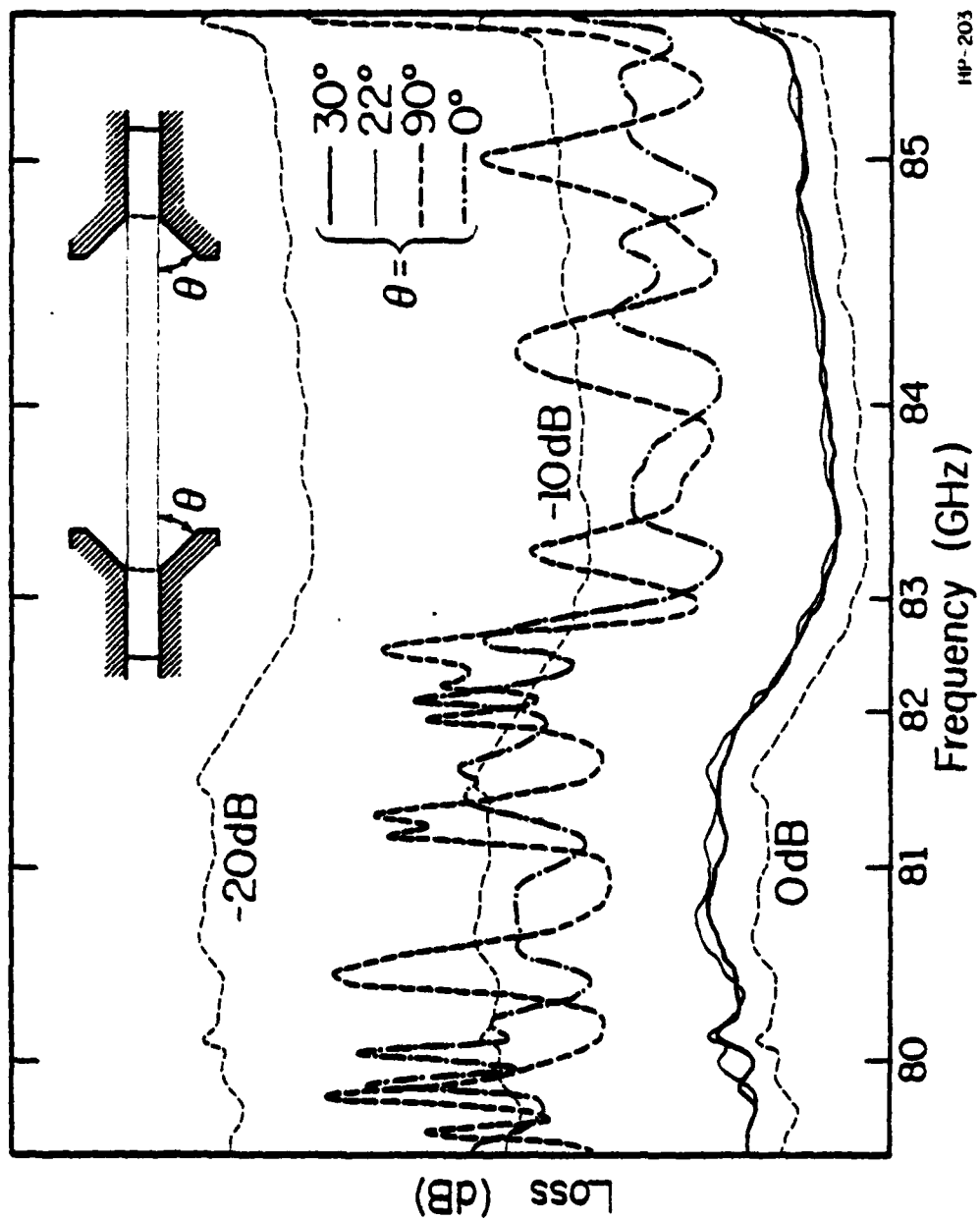
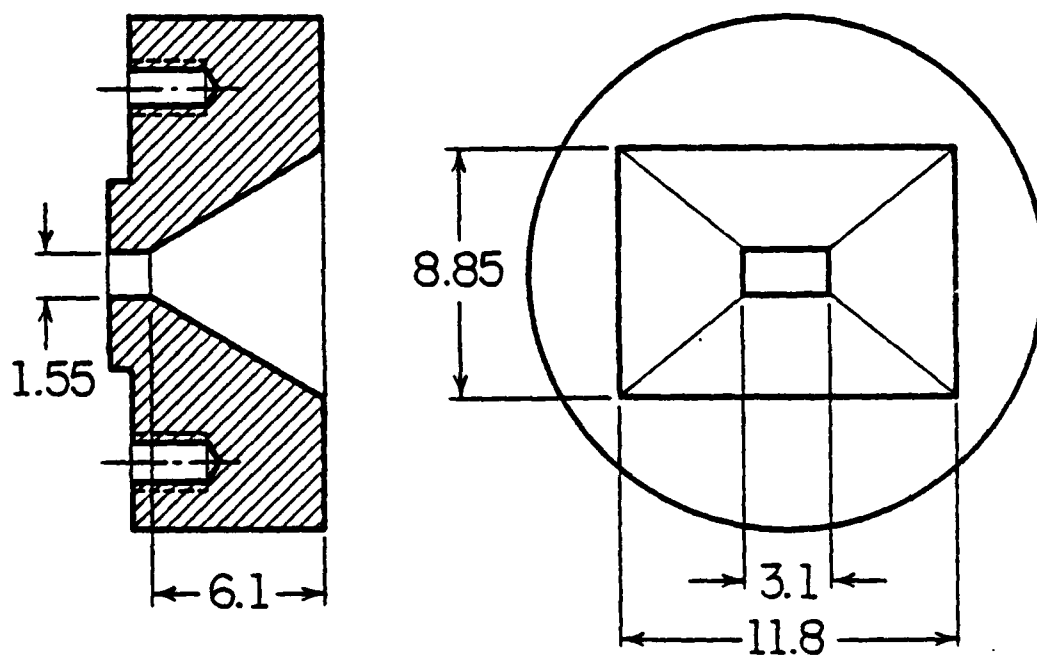


Figure 7. Total Insertion Loss



HP-209

Figure 8. Dimensions of the Designed Horn

by adding independent circuit elements, such as tuning or active devices, without further increasing the loss to the circuit. Another important application is the excitation of the integrated dielectric antennas which is illustrated with the example of a slow-wave dielectric rod antenna excited by a metal waveguide.

As may be expected, an inefficient transition causes undesirably high side lobes to appear in the radiation pattern of the antenna. To demonstrate the significant improvement achieved by the use of a well-designed transition, the radiation pattern of a slow-wave dielectric rod antenna of 40 mm ($\sim 11 \lambda_0$) in length excited by the transition horn described above was compared to the radiation pattern of the same antenna excited by an ordinary truncated metal waveguide. The results are shown in Figure 9. The antenna with the horn launcher has more than 2 dB gain over the same antenna using the ordinary truncated launching waveguide. Moreover, the side lobes due to feed end radiation of the antennas excited by an ordinary launcher are very high.

For a 25 mm long dielectric rod antenna, if the transition horn is employed, the directive gain is about 24 dB and the side lobe suppression is clearly evident. Again, due to the feed end radiation, the main beam of the antenna excited by the truncated metal waveguide is distorted, and the side lobes are high. This is shown in Figure 10.

It is also interesting to observe that the metal horn, when used as an antenna, has lower directive gain than the short dielectric antenna using the same metal horn as a launcher. The null-to-null beam width of the metal horn is about 40 degrees broader than the dielectric antenna employing the metal horn launcher. This is shown in Figure 11.

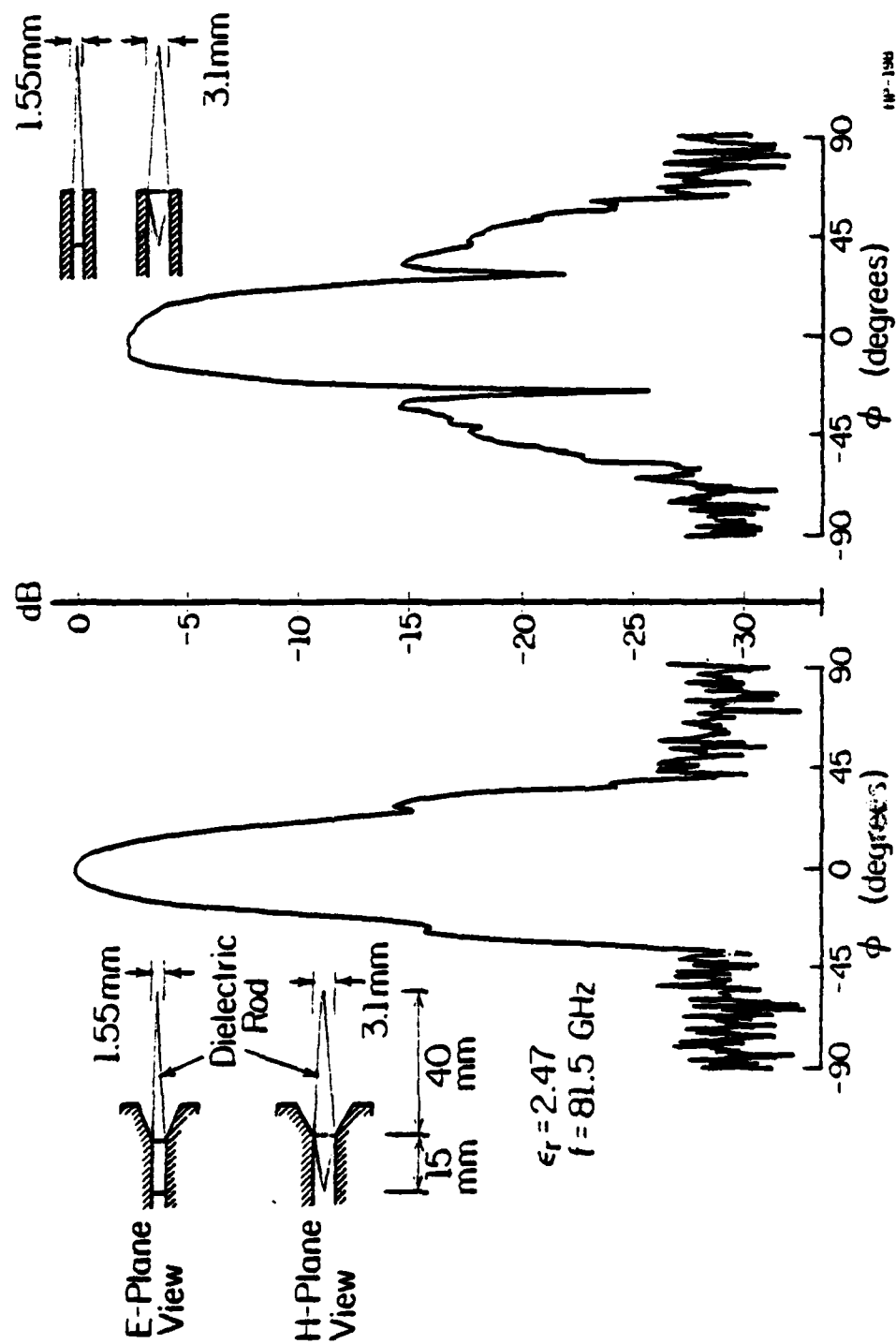


Figure 9. Comparison of Radiation Patterns in the H-Plane for a Dielectric Antenna Using Two Types of Transitions

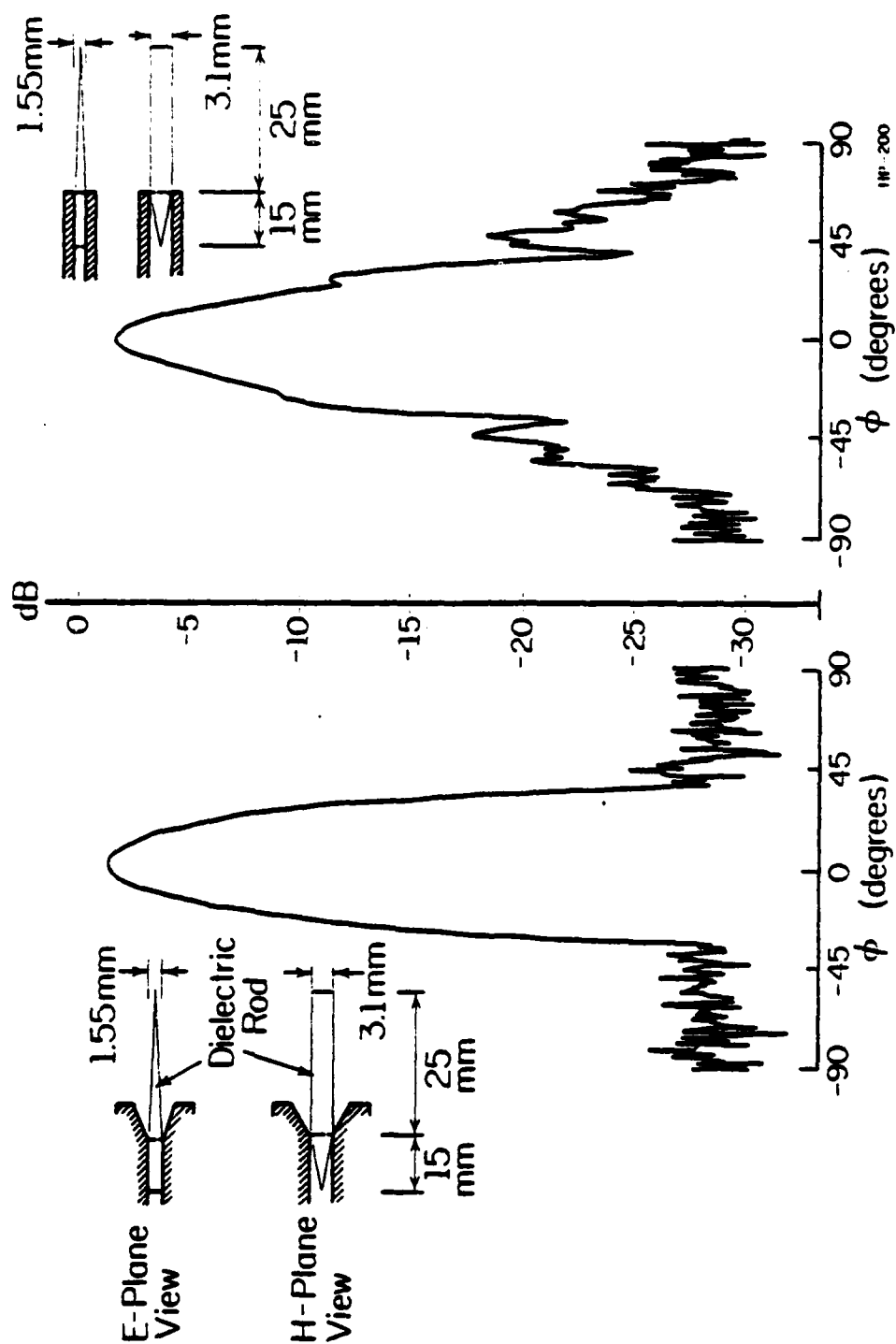


Figure 10. Comparison of Radiation Patterns in the H-Plane for a Dielectric Antenna Using Two Types of Transition

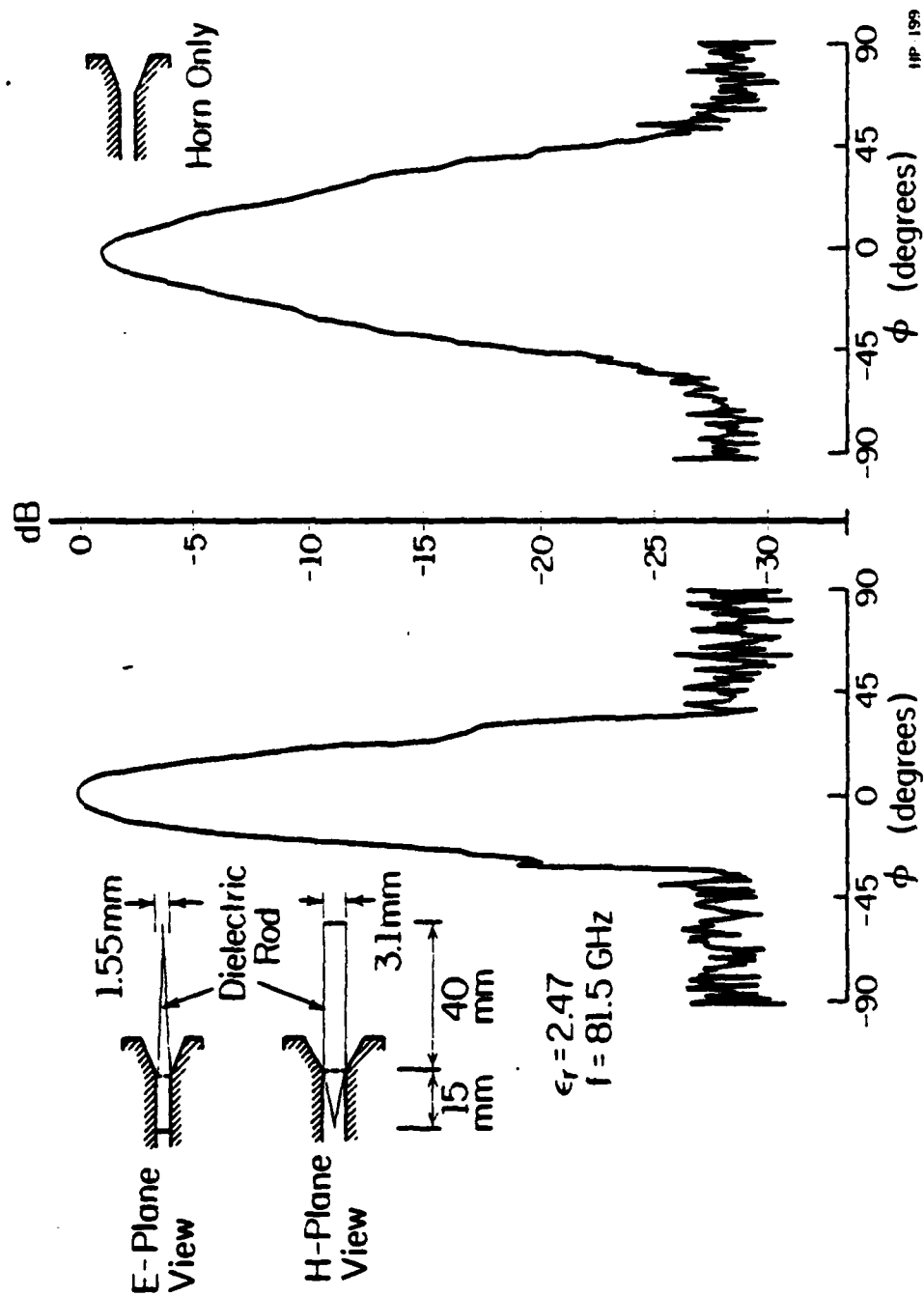


Figure 11. Comparison of Radiation Patterns of the Metal Horn and the Short Dielectric Antenna Using the Same Metal Horn as Transition

III. COUPLING CHARACTERISTICS OF DIELECTRIC WAVEGUIDES

A typical millimeter-wave integrated circuit is shown in Figure 12 [8]. It contains an oscillator, a balanced mixer, a 10 dB and a 3 dB directional coupler, a band reject filter and a channel dropping filter. The port 2 can be connected to an antenna or to another millimeter-wave integrated circuit either directly or with the help of the metal-to-dielectric transitions described in the previous chapter. In this circuit, it is easy to recognize that the filters (or resonators) consist of several directional couplers themselves, since part of the band reject filter is a nonsymmetric coupler, and the channel dropping filter consists of two nonsymmetric couplers and a non-uniform spacing symmetric coupler. Hence, apart from the active devices, the dielectric directional couplers play an extremely important role in a millimeter-wave integrated circuit. For this reason, it is necessary to study the coupling characteristics of these couplers in great detail. Only the dielectric waveguide structure is discussed here although the same analyses can be directly applied to other guiding structures such as image guide, inverted strip or insular guide.

A. Simple Distributed Directional Couplers

Consider the cross-sectional view of the coupled structure at the plane $z = 0$ in Figure 13. The symmetry about the $x = 0$ plane suggests that the fields are either symmetric or antisymmetric with respect to that plane. Consequently, as shown in Reference 2, the propagating modes of the coupled structure are either symmetric (k_{even}) or antisymmetric (k_{odd}). Assuming that fundamental E_{11}^y mode is launched from a conventional metal waveguide, the two wave numbers k_{even} and k_{odd} are given by

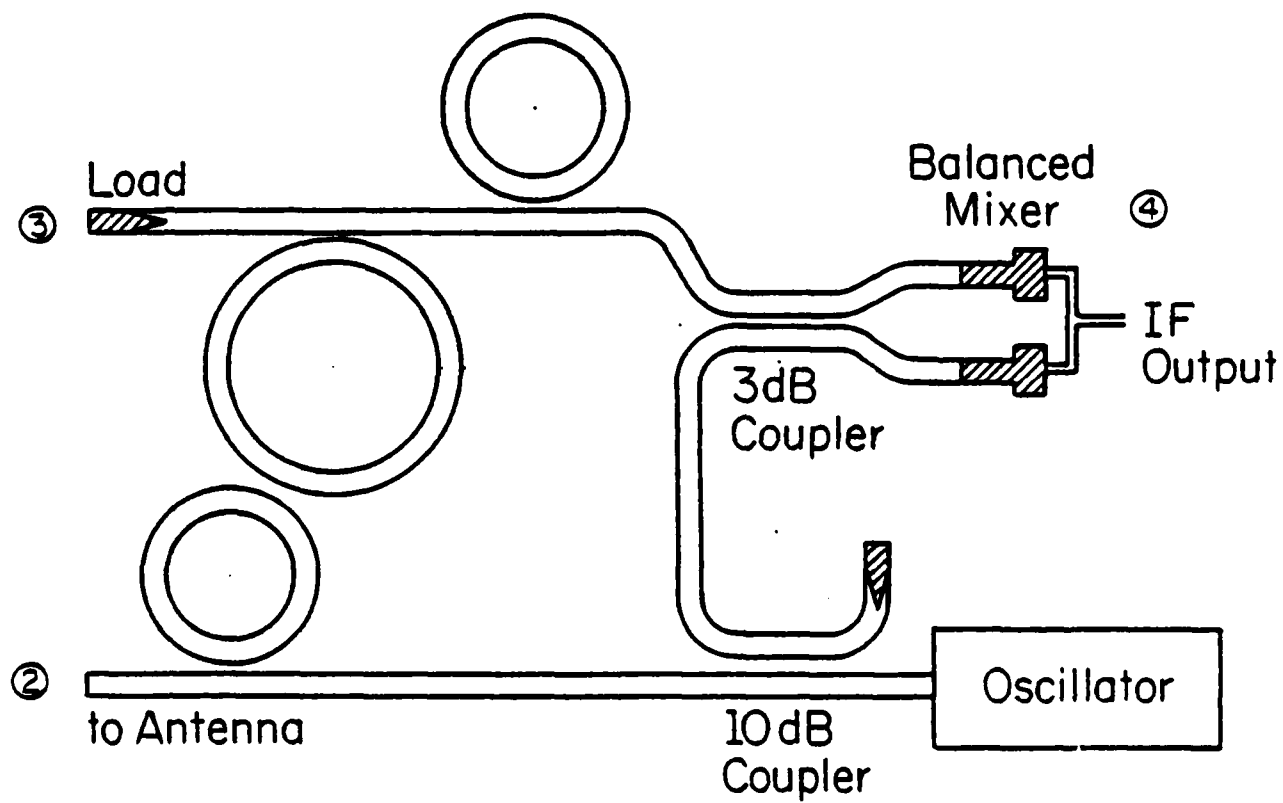
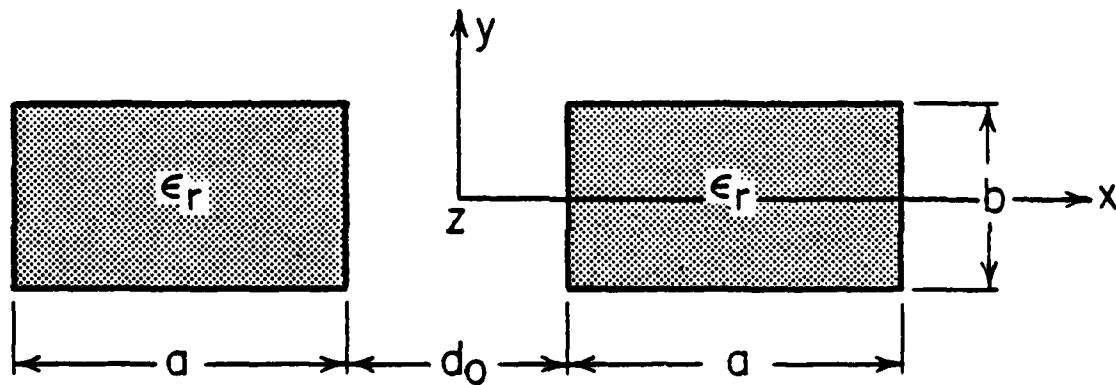


Figure 12. Typical Millimeter-Wave Integrated Circuit



$$\begin{aligned}\epsilon_r &= 2.6 \\ a &= 2.27 \text{ cm} \\ b &= 1.00 \text{ cm}\end{aligned}$$

HP-208

Figure 13. Cross-Sectional View of the Coupled Structure

$$\left. \begin{matrix} k_{\text{even}} \\ k_{\text{odd}} \end{matrix} \right\} = k_z \left\{ 1 \pm 2 \frac{k_x^2 \xi \exp(-d/\xi)}{k_z^2 a (1 + k_x^2 \xi^2)} \right\} \quad (1)$$

where k_x and k_z are the transverse and longitudinal propagation constants of a single guide, respectively, and can be derived using the generalized effective dielectric constant method (see Appendix A); d is the spacing between the two guides; and ξ is the field decay coefficient, i.e., the distance over which the fields decay by e^{-1} .

$$\xi = ((\epsilon_{re} - 1)k_0^2 - k_x^2)^{-\frac{1}{2}} \quad (2)$$

In expression (2), the relative dielectric constant of the material has been replaced by the effective dielectric constant which is given as

$$\epsilon_{re} = \epsilon_r - (k_y/k_0)^2 \quad (3)$$

k_y is also obtained by the generalized effective dielectric constant method.

It should be mentioned that in a recent paper by the same authors [9], two values of ξ had to be determined, and more approximations were made. The approach used here is believed to be superior.

A simple distributed directional coupler of length l is shown in Figure 14. The port numbers are defined by the usual convention. Since, in a coupled structure, it is the interaction of the symmetric and antisymmetric modes of the propagation constants that induces the coupling between the two dielectric waveguides [2], the scattering coefficients for the coupling section can be expressed as (see Appendix B)

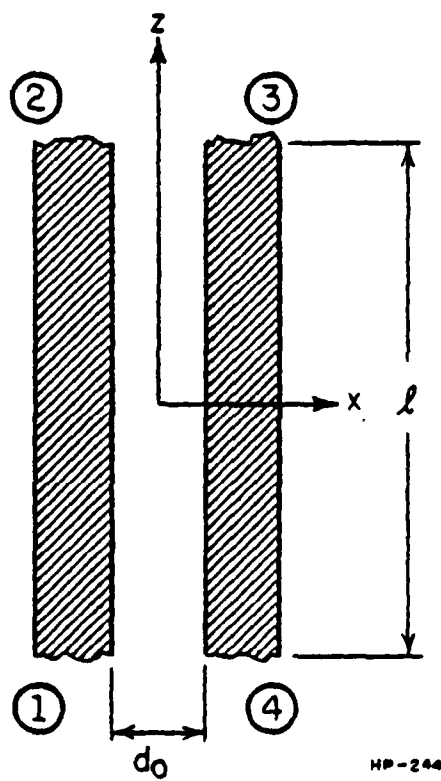


Figure 14. Simple Distributed Directional Coupler

$$|S_{31}| = \left| \sin\left(\frac{k_{\text{even}} - k_{\text{odd}}}{2} l\right) \right| \quad (4)$$

$$|S_{21}| = \left| \cos\left(\frac{k_{\text{even}} - k_{\text{odd}}}{2} l\right) \right| \quad (5)$$

where l is the total coupling length of the coupling section; and $(k_{\text{even}} - k_{\text{odd}})/2$ is defined as the coupling coefficient. It is obvious that the larger the coupling coefficient, the stronger the degree of coupling between the two guides.

B. Analyses of Practical Coupling Structures

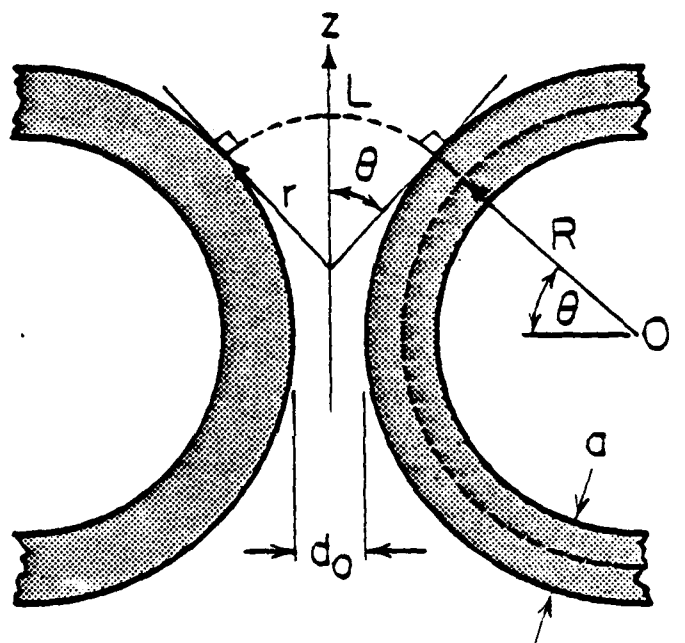
B.1. Nonuniform Spacing Symmetric Couplers

In practice, most of the coupling structures are more complicated than the simple distributed directional coupler described in the previous section. One of the popular configurations is the symmetric coupler with nonuniform coupling spacing as shown in Figure 15.

For the radius R sufficiently large, the wave numbers of both guides can be assumed to be identically equal to that of a straight guide. In a dielectric waveguide, the equiphase fronts of the propagating modes are normal to the axial propagation direction. We assume that, with the existence of the second dielectric guide, these fronts are cylindrical planes. Consequently, the separation distance between the incremental coupling lengths of the two lines is given by the arc length L . The total coupling of the two lines is the summation of the coupling from these incremental coupling lengths. The spacing d in (1) is replaced by L , which for the symmetric structure of Figure 15, is given by

$$L = 2r\theta \quad (6)$$

where θ is the angle from the incremental coupling length to the center



HP-196

Figure 15. Non-Uniform Spacing Symmetric Coupler

line; r is the radius of the cylindrical phase fronts which can be expressed as a function of θ as

$$r = \frac{d_0 + 2(R + a/2)(1 - \cos\theta)}{2\sin\theta} \quad (7)$$

where d_0 is the smallest spacing between two curved dielectric guides.

The scattering coefficients can be derived by substituting (6), (7) and (1) into (4) and (5) and using $l = Rd\theta$ to get

$$|S_{31}| = |\sin(KI_s)| \quad (8)$$

and

$$|S_{21}| = |\cos(KI_s)| \quad (9)$$

where

$$K = \frac{4k_x^2 \xi R}{k_z a (1 + k_x^2 \xi^2)} \quad (10)$$

and

$$I_s = \int_0^{\pi/2} \exp\left[-\frac{\theta\{d_0 + 2(R + a/2)(1 - \cos\theta)\}}{\xi \sin\theta}\right] d\theta. \quad (11)$$

In these equations, the integral form has been used for the summation of the couplings from all incremental coupling lengths. The experimental and calculated results of $|S_{21}|$ and $|S_{31}|$ as a function of the spacing d_0 are plotted together as shown in Figures 16 and 17. The guide dimensions are shown in Figure 13.

B.2. Nonsymmetric Couplers

Another very important class of dielectric couplers is the nonsymmetric coupler shown in Figure 18 where ports 1 and 2 are connected by a straight dielectric guide, 3 and 4 by a curved dielectric guide.

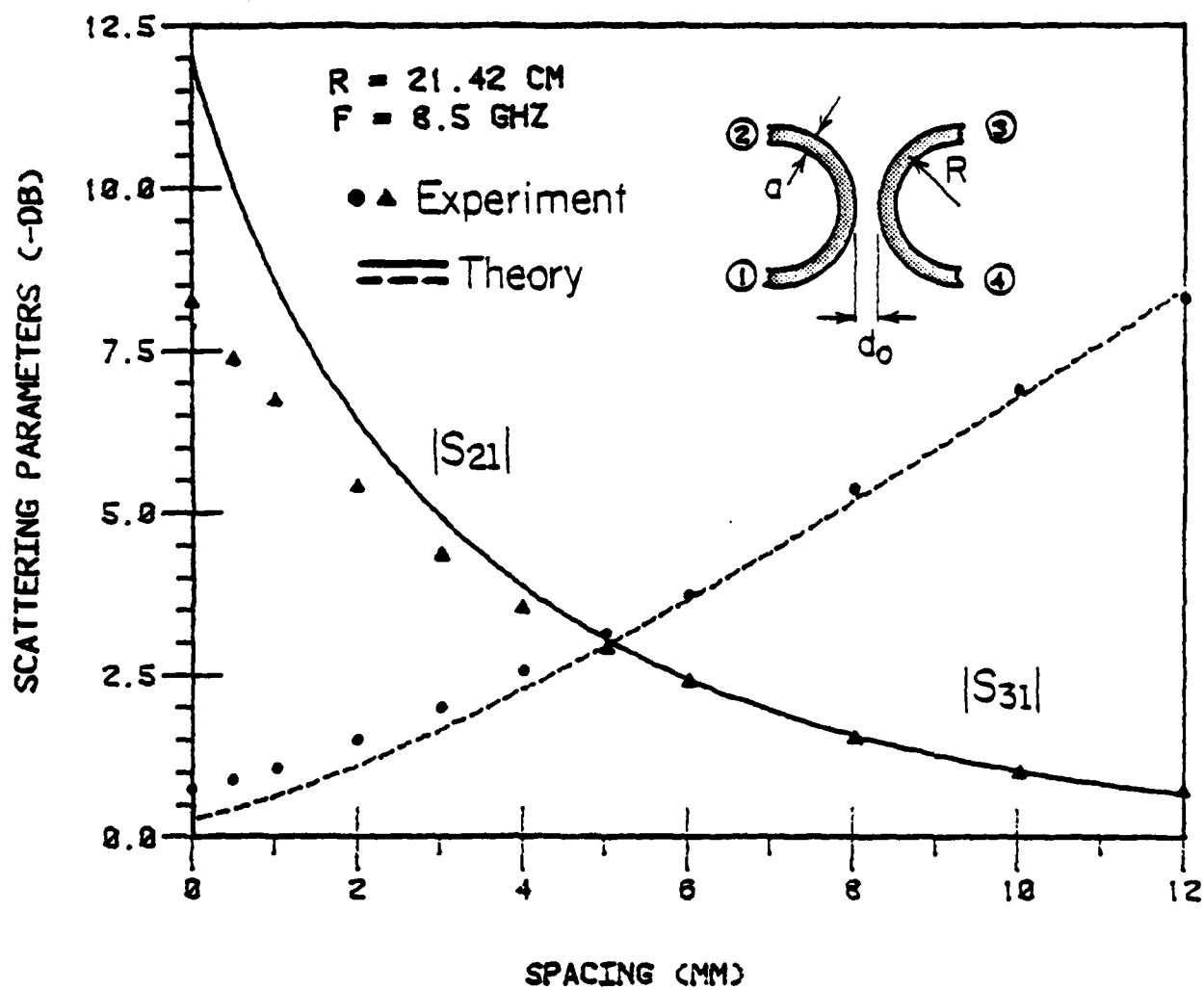


Figure 16. Scattering Coefficients of a Symmetric Coupler vs. Guide Spacing d_0 at $f = 8.5 \text{ GHz}$

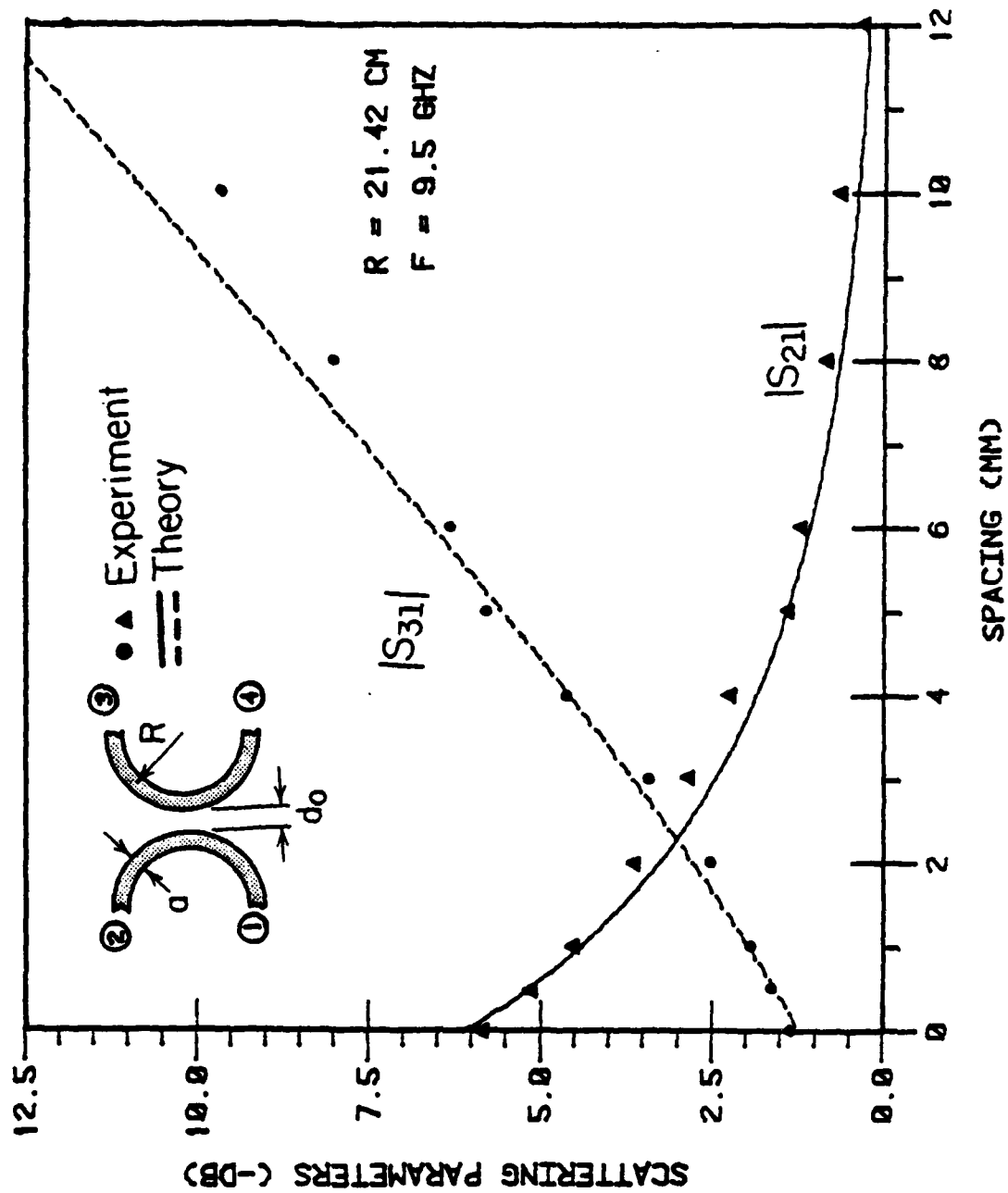


Figure 17. Scattering Coefficients of a Symmetric Coupler vs. Guide Spacing d_0 at $f = 9.5 \text{ GHz}$

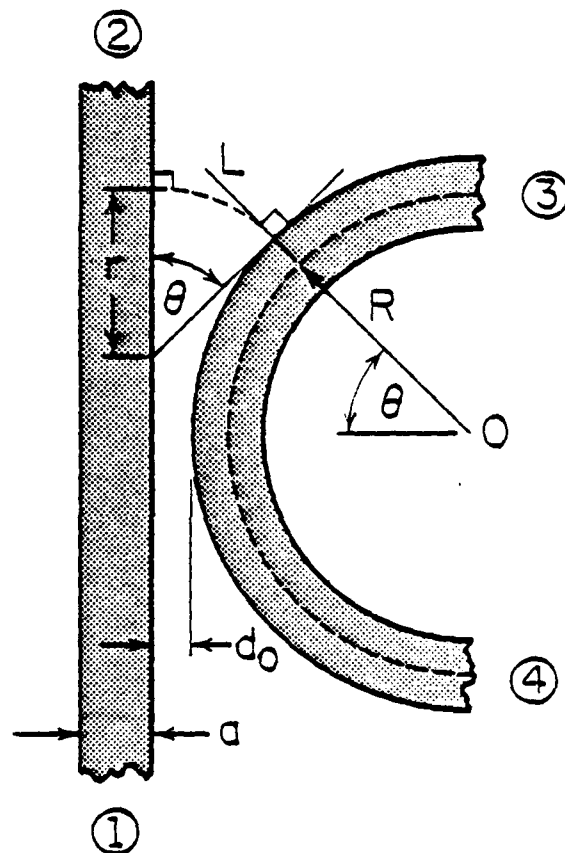


Figure 18. Non-Symmetric Coupler

The energy is excited at port 1. Using the same arguments as before, i.e., the wavefronts are normal to the axial propagation direction and these fronts are cylindrical planes, the separation distance between the incremental coupling lengths of a nonsymmetric coupler becomes

$$L = r\theta \quad (13)$$

where

$$r = \frac{d_0 + (R + a/2)(1 - \cos\theta)}{\sin\theta} \quad (14)$$

The integral expression for the summation of the couplings of all incremental lengths for this structure can be expressed as

$$I_n = \int_0^{\pi/2} \exp\left[-\frac{\theta\{d_0 + (R + a/2)(1 - \cos\theta)\}}{\xi \sin\theta}\right] d\theta \quad (15)$$

Up to this point, the coupling coefficient for the nonsymmetric coupler is derived using the assumption that the propagation constants of the curved and straight dielectric guides are identical. For most practical cases, this assumption is not valid. The difference in the propagation constants of the two guides will inevitably degrade the coupling coefficient which so far is assumed to be ideal. Experimental values of the coupling coefficient are always much less than the theoretical values. Hence, it is necessary to multiply the derived coupling coefficient by a correction factor v . The scattering coefficients for a nonsymmetric coupler become

$$|S_{31}| = |\sin(vKI_n)| \quad (16)$$

$$|S_{21}| = |\cos(vKI_n)| \quad (17)$$

where v is determined from experiment and, in general, depends on the operating frequency and the curvature of the curved guide. For a given frequency, it is fortunate that only one simple experiment is necessary to determine v (usually on S_{21} since it is easy to measure). Once obtained, the same value can be used for all other computations. For most practical cases, v varies in the range from 0.5 to 0.7. Table 1 shows some typical values of v for different frequencies and radii of curvature. Higher values of v correspond to higher operating frequencies and larger radii of curvature. Figures 19 and 20 compare the experimental and the calculated results for the scattering coefficients at various frequencies as a function of the guide spacing d_0 .

B.3. Coupling Structure Incorporating a Straight Coupling Section with Two Nonsymmetric Curved Arms

Sometimes it is desirable to design a coupling structure that is capable of transferring all energy from one guide to the other. The two structures described in the previous sections by themselves do not have that capability unless the radius of the curved guides becomes prohibitively large. The coupling can greatly be improved if a straight dielectric waveguide section of length l_0 is inserted between two curved connecting arms. The structure with symmetric connecting arms has been investigated by other authors [6] and is not mentioned again.

The coupling structure in which a straight coupling section l_0 is inserted between two nonsymmetric curved dielectric guides is shown in Figure 21. Port 1 to 2 is a straight guide; from 4 to 3 is a straight guide inserted between two curved dielectric guides. Since the field distributions at the junction between the curved and straight guides have to be continuous, the total coupling of the structure is

TABLE 1

TYPICAL VALUES OF THE CORRECTION FACTOR
 ν FOR NONSYMMETRIC COUPLERS

Radius (cm)	Frequency (GHz)	Correction Factor
18.9 ($R/a = 8.3$)	8.5	0.58
	9.0	0.63
	9.5	0.64
	10.0	0.69
21.42 ($R/a = 9.43$)	8.5	0.56
	9.0	0.61
	9.5	0.64
	10.0	0.68
23.96 ($R/a = 10.55$)	8.5	0.55
	9.0	0.61
	9.5	0.64
	10.0	0.68

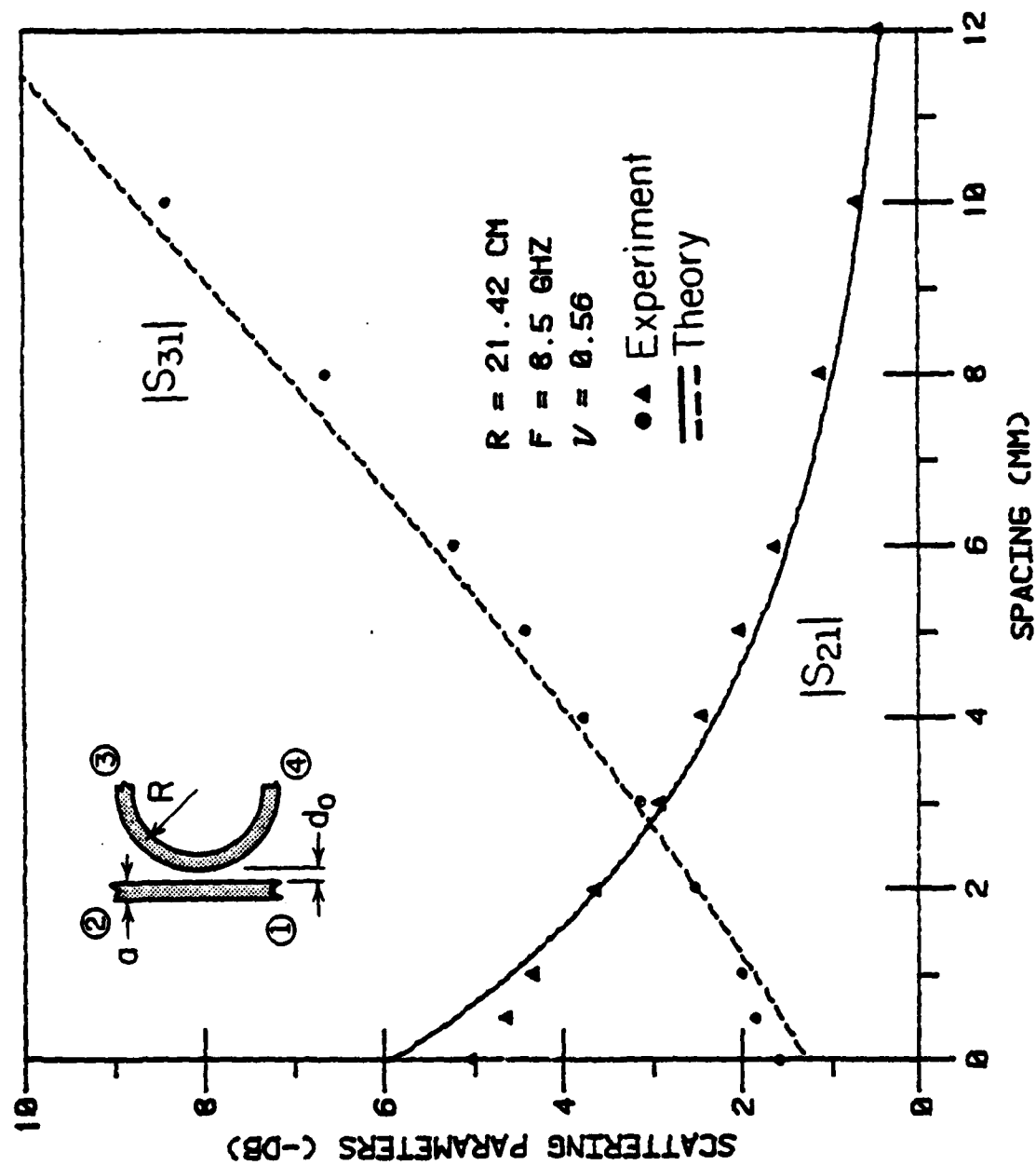


Figure 19. Scattering Coefficients of a Non-Symmetric Coupler vs. Guide Spacing d_0 at $f = 8.5 \text{ GHz}$

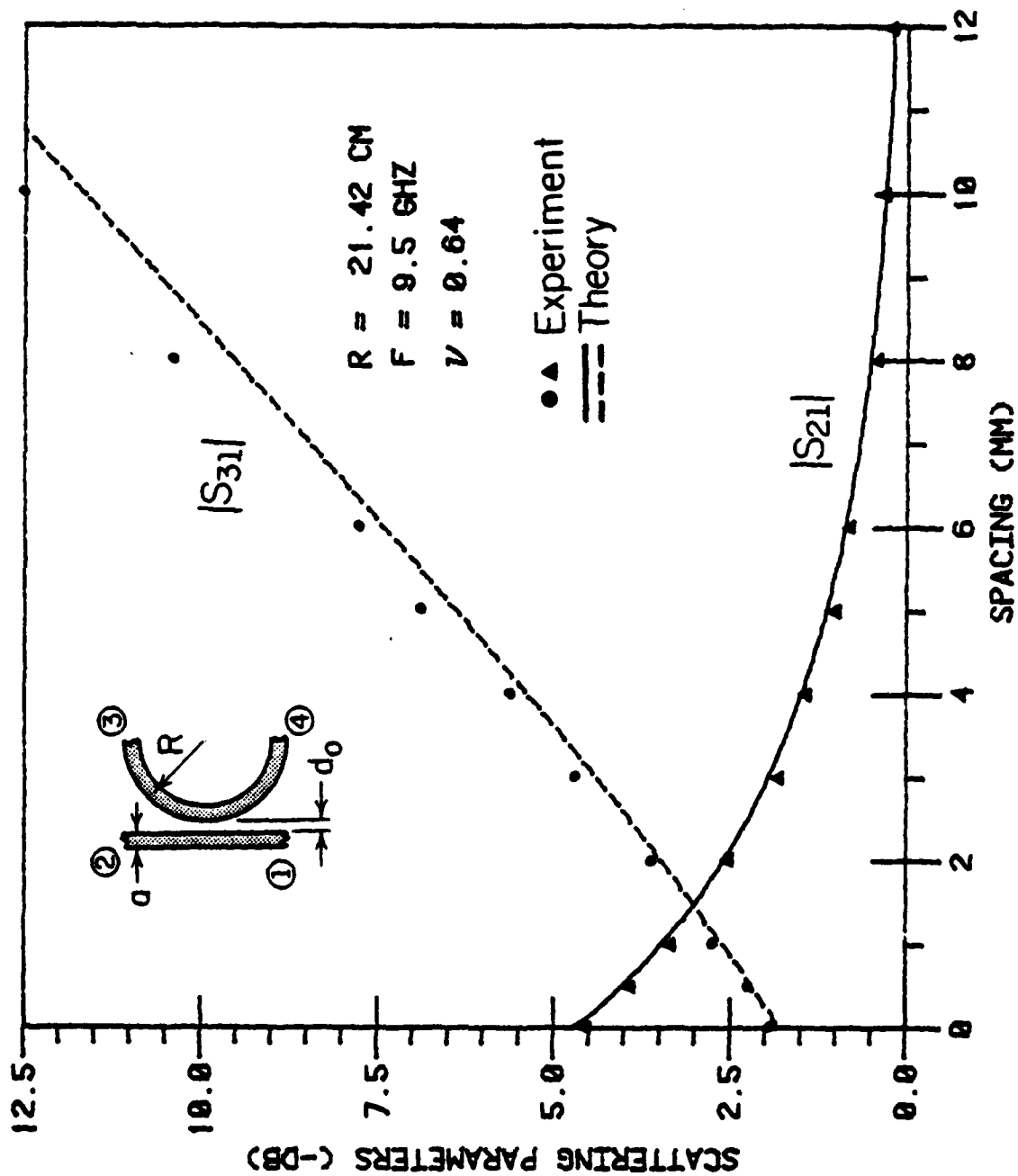


Figure 20. Scattering Coefficients of a Non-Symmetric Coupler vs. Guide Spacing d_0 at $f = 9.5 \text{ GHz}$

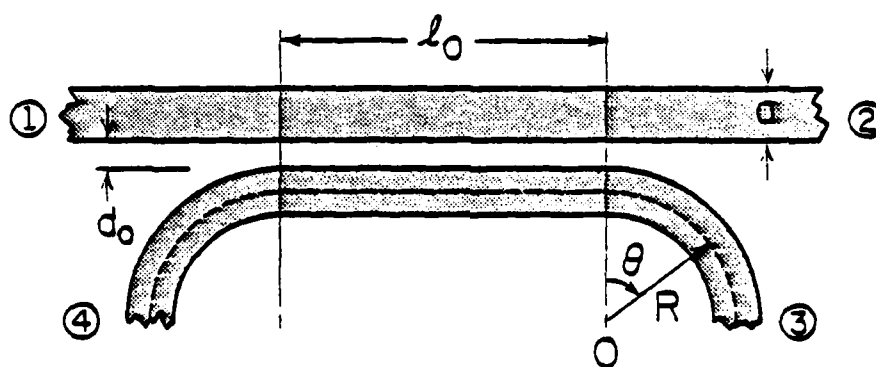


Figure 21. Coupling Structure Incorporating a Straight Section and Curved Connecting Arms

the sum of the coupling from the straight section and that from the curved connecting arms. Consequently, the scattering coefficients for this structure become

$$|S_{31}| = \left| \sin v \left(\frac{k_{\text{even}}(s) - k_{\text{odd}}(s)}{2} \ell_0 + \frac{k_{\text{even}}(c) - k_{\text{odd}}(c)}{2} \ell \right) \right| \quad (18)$$

and
$$|S_{21}| = (1 - |S_{31}|^2)^{\frac{1}{2}} \quad (19)$$

where v is the same correction factor that was obtained for a non-symmetric coupler (see Section B.2). In Equation (18), the first term inside the argument is for the uniform spacing section, and the second term is for the nonsymmetric coupler.

If k_{even} and k_{odd} are substituted into (18), the scattering coefficients can be rewritten in the form

$$|S_{31}| = \left| \sin \left(v K \left\{ \frac{e^{-d_0/\xi}}{2R} \ell_0 + I_n \right\} \right) \right| \quad (20)$$

The experimental and calculated results of $|S_{21}|$ and $|S_{31}|$ as a function of the guide spacing d_0 are plotted together and are shown in Figures 22 and 23.

C. Experimental Verifications

Experiments were carried out in X-band because the component sizes are more manageable and the measurements are more accurate. To reduce the effect of the large mismatch caused by reflection and radiation in normal launching devices, the fundamental E_{11}^y mode was launched from an improved rectangular horn as described in Chapter I.

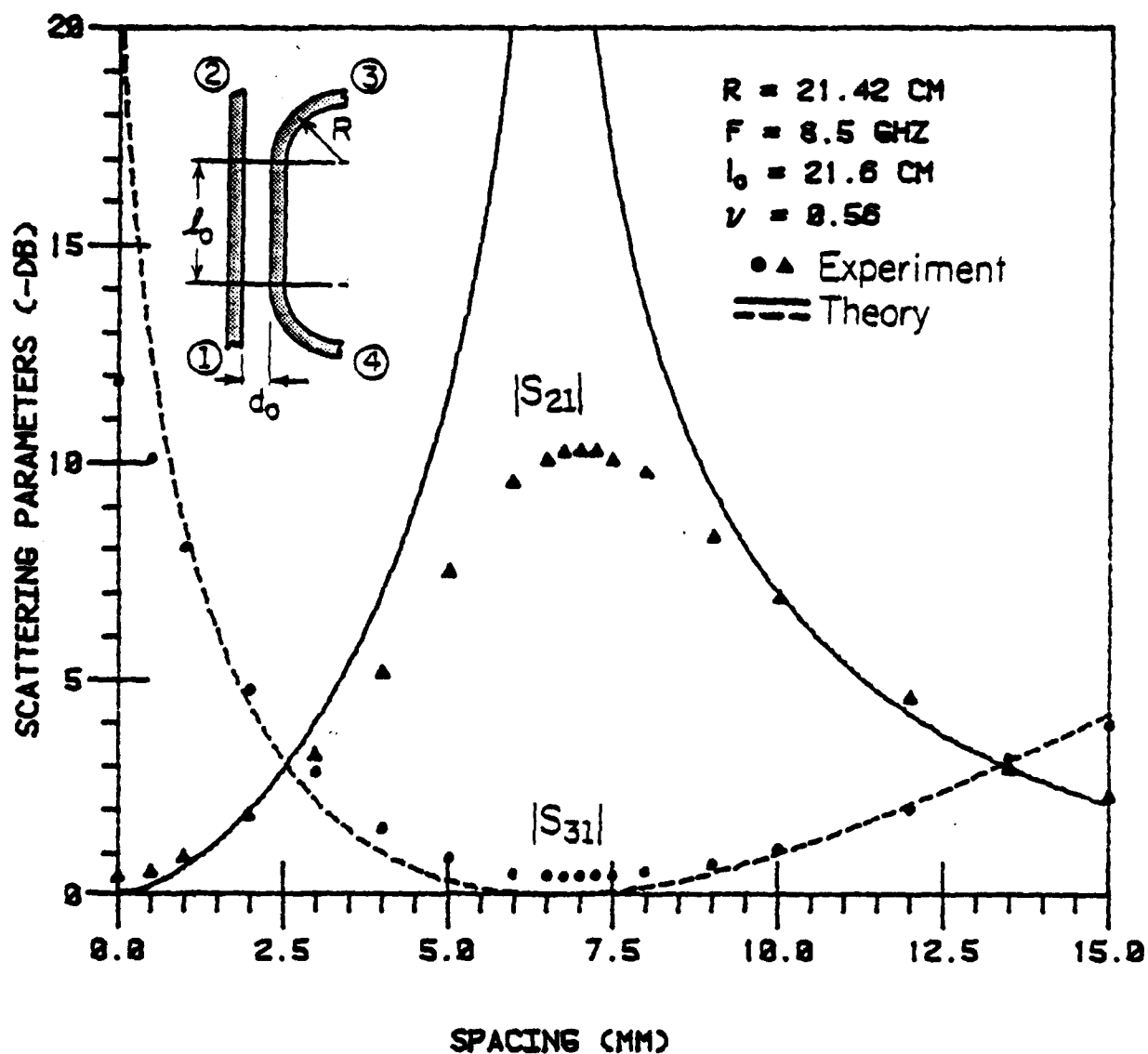


Figure 22. Scattering Coefficients of the Coupler Shown in Fig. 21 for $f = 8.5 \text{ GHz}$

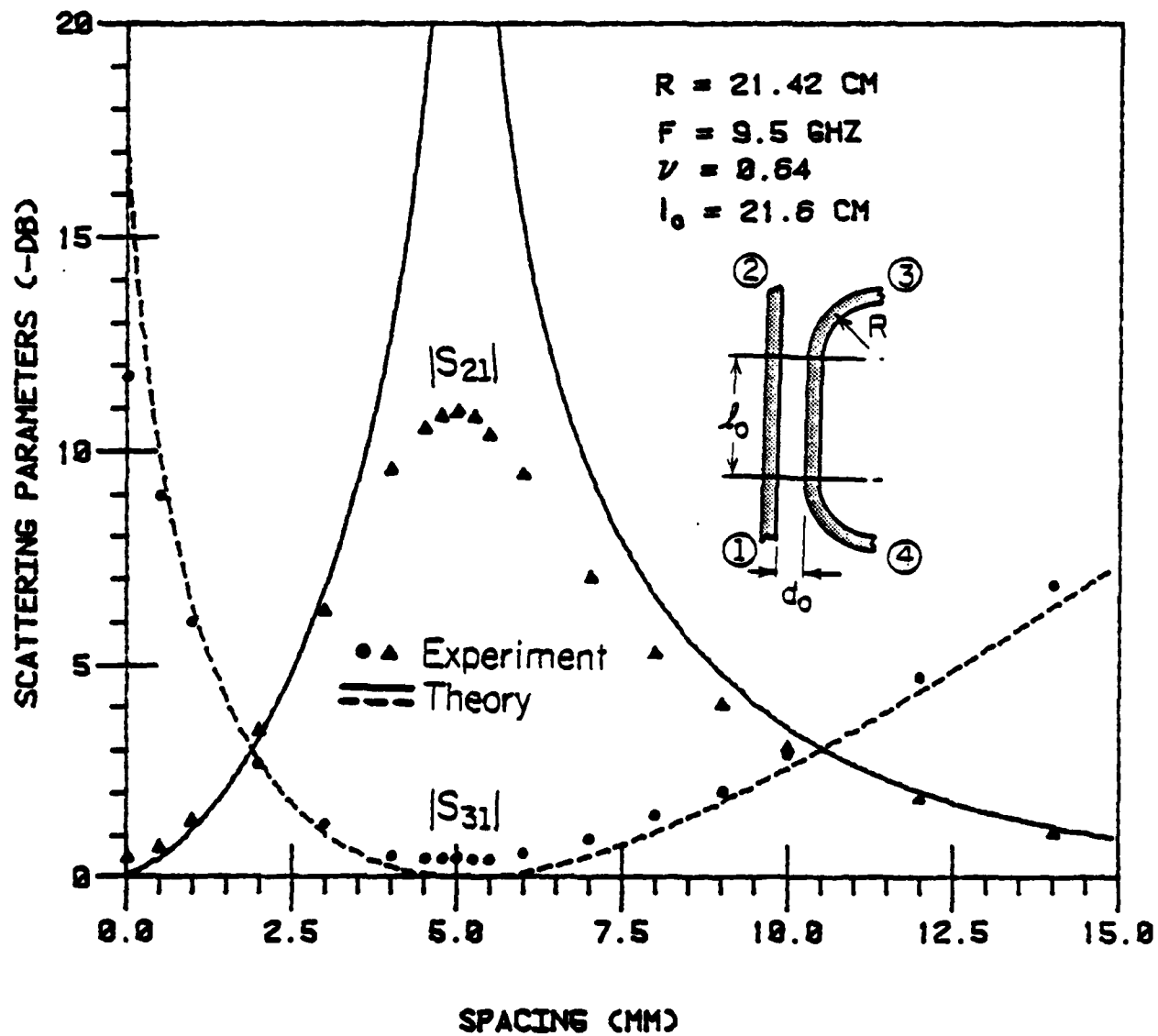


Figure 23. Scattering Coefficients of the Coupler Shown in Fig. 21 for $f = 9.5 \text{ GHz}$

The guiding media were fabricated from plexiglass ($\epsilon_r \approx 2.6$). The curved sections were made sufficiently large to reduce the effect of radiation since the purpose of this investigation is to study the coupling characteristics only. The whole structure is supported by bubble styrofoam ($\epsilon_r \approx 1$) and surrounded by absorbers to eliminate stray radiation.

The propagation constant of the single guide was determined by the generalized effective dielectric constant method. It is interesting to note that for a symmetric coupler even though the separation between the two guides is larger than for a nonsymmetric coupler, the coupling of the symmetric coupler is more pronounced than the latter one. Also, for a given radius of curvature, the coupling is decreased by increasing frequency.

For the coupling structure where a straight section is inserted between two curved arms, we still have to multiply the coupling coefficient by a correction factor v in order to match the experimental and theoretical results. In all experiments, if the energy is excited at port 1 of the straight guide, the correction factor for the straight section assumed the same value as that for a nonsymmetric coupler. This is desirable since only a very simple measurement is made to obtain a value for the correction factor, and this value is used for all computations of both structures. The multiplication of the coupling coefficient of the straight section of the coupling structure in Figure 21 by a correction factor, which for most practical applications varies between 0.5 to 0.7 (see Table I) shows that the coupling of a nonuniform spacing symmetric coupler is very strong. The reason for this is the fields at the convex side of each curved guide decay very slowly and extend very far into the air medium. As a result,

the interaction between the propagating modes is very strong. For a nonsymmetric coupler and the coupling structure shown in Figure 21, apart from the fact that the propagation constants in each guide are different, the fields outside the straight guide decay so fast that the interaction between the propagating modes becomes minimal.

Scattering coefficients of various coupling structures were measured and compared with calculated results. Experimental results agree well with calculated values throughout. The scattering coefficient $|S_{41}|$ has been ignored in all figures since it is less than 25 dB for all measurements.

IV. CONCLUSIONS

A small, low loss and easy to fabricate metal-to-dielectric waveguide transition has been designed for applications in millimeter-wave integrated circuits and antennas. Since no dimensions are critical, manufacturing is inexpensive. The loss figure of less than 0.5 dB per transition has been obtained for a broad frequency range with a relatively small transition length.

With the use of these transitions to reduce the radiation from the feed end of dielectric guides that may interfere with the normal operation of the dielectric components, the coupling characteristics of various structures were accurately investigated experimentally and theoretically. For a nonsymmetric coupler, it is only necessary to make one simple experiment to determine the correction factor for the coupling coefficient. Once obtained, this value can be used for all other computations. Comparisons of calculated and measured scattering coefficients are very good.

V. APPENDICES

A. Appendix A: Generalized Effective Dielectric Constant Method

In the past, several authors have attempted to find the exact solutions for the propagation constants of a dielectric waveguide [10], [11] using infinite systems of linear equations. For many applications, these approaches are impractical since they needlessly require too much computation. Unless a very large number of terms are used, the result can be doubtful.

A simple analytical approach for calculating the propagation constants was introduced by Marcatili [2]. In his analysis, the transverse propagation constants were obtained by assuming that the dielectric waveguide can be treated as a homogeneous slab in both the x- and y-directions. Therefore, k_x and k_y can be obtained independently. If the surrounding medium is assumed to be free space, the transverse propagation constants for the E_{pq}^y modes are solutions of the eigenvalue equations

$$k_y b = q\pi - 2 \tan^{-1} \left(\frac{k_y \eta}{\epsilon_r} \right) \quad (A-1)$$

$$k_x a = p\pi - 2 \tan^{-1} (k_x \xi) \quad (A-2)$$

in which

$$\eta = ((\epsilon_r - 1)k_0^2 - k_y^2)^{-\frac{1}{2}} \quad (A-3)$$

$$\xi = ((\epsilon_r - 1)k_0^2 - k_x^2)^{-\frac{1}{2}} \quad (A-4)$$

where ϵ_r is the relative permittivity of the dielectric material, and η and ξ are the field decay coefficients in the y and x direction, respectively.

However, this simple approximation failed to predict the propagation of the fundamental mode at low frequencies. The effective dielectric constant method [12] was considered a slight modification to Marcatili's approach.

In the new method, k_x and k_y are related through the effective dielectric constant and the eigenvalue equations. Since this concept has been studied extensively elsewhere, only a brief discussion is given here.

Consider a rectangular dielectric waveguide extending to $\pm \infty$ in the x direction as a dielectric slab. The eigenvalue equation (A-1) for k_y is obtained by matching the tangential field components at $y = \pm b/2$. Once obtained, this transverse propagation constant k_y is assumed to be the same as that of the original dielectric waveguide. Since it has been transformed into a slab in x, the dispersion relation becomes

$$k_z^2 = \epsilon_r k_0^2 - k_y^2 = k_0^2 + \eta^2 \quad (\text{A-5})$$

and from this equation, the effective dielectric constant ϵ_{rey} is defined as

$$\epsilon_{\text{rey}} = \left(\frac{k_z}{k_0} \right)^2 = \epsilon_r - \left(\frac{k_y}{k_0} \right)^2 \quad (\text{A-6})$$

The dielectric waveguide is now transformed again into an infinitely long slab in y with the relative dielectric constant replaced by the effective dielectric constant (A-6) which takes into account the propagation in the y-direction.

The eigenvalue equation for k_x which is obtained by matching the tangential field components, is shown as Equation (A-2) with

ξ replaced by ξ_{eff} where

$$k_z^2 = \epsilon_{\text{rey}} k_0^2 - k_x^2 = k_0^2 + \xi_{\text{eff}}^2 \quad (\text{A-7})$$

and

$$\xi_{\text{eff}} = ((\epsilon_{\text{rey}} - 1)k_0^2 - k_x^2)^{-\frac{1}{2}} \quad (\text{A-8})$$

In short, k_x was obtained from k_y through the effective dielectric constant ϵ_{rey} , and the longitudinal propagation constant of the original waveguide is given by

$$k_z^2 = \epsilon_r k_0^2 - k_x^2 - k_y^2 \quad (\text{A-9})$$

Obviously, this sequence can be reversed by first transforming the dielectric waveguide into a slab in y with the dispersion relation

$$k_z^2 = \epsilon_r k_0^2 - k_x^2 = k_0^2 + \xi^2 \quad (\text{A-10})$$

from which the new effective dielectric constant is obtained

$$\epsilon_{\text{rex}} = \left(\frac{k_z}{k_0}\right)^2 = \epsilon_r - (k_x/k_0)^2 \quad (\text{A-11})$$

where k_x is obtained from Equations (A-2) and (A-4).

With the new effective dielectric constant for the transformed dielectric waveguide to compensate for the propagation in x , the dielectric waveguide is now extended to a slab in x with the relative permittivity replaced by the new effective permittivity ϵ_{rex} . The transverse propagation constant k_y is the solution of the following eigenvalue equation

$$k_y b = q\pi - 2 \tan^{-1} \left(\frac{k_y \eta_{\text{eff}}}{\epsilon_{\text{rex}}} \right) \quad (\text{A-12})$$

and η_{eff} is obtained from the following dispersion relation:

$$k_z^2 = \epsilon_{\text{rex}} k_0^2 - k_y^2 = k_0^2 + \eta_{\text{eff}}^2. \quad (\text{A-13})$$

Hence, for this sequence, k_y is indirectly related to k_x through the effective dielectric constant ϵ_{rex} . The new sequence of the effective dielectric constant just described above is believed to be equivalent to the effective permeability derived by other authors [13], [14] through different procedures and explanations.

Since each method has its own merit, and k_x and k_y are related through either ϵ_{rex} or ϵ_{rey} , it may be desirable to combine these two approaches to obtain a "generalized" effective dielectric constant method. To do so, the dielectric waveguide was first transformed into a dielectric slab in the x direction and k_{y1} was obtained by using Equations (A-1) and (A-3). k_{x1} is then obtained from k_{y1} using the effective dielectric constant ϵ_{rey} . So far, it is the original effective dielectric constant method described by Knox and Toullos. However, a new value k_{y2} is obtained from k_{x1} using the effective dielectric constant ϵ_{rex} . These steps were described from Equations (A-10) to (A-13). Then k_{x2} is obtained from k_{y2} using the effective dielectric constant ϵ_{rey} again, and so on. After a few iterations, the transverse propagation constants k_x and k_y will converge, and from which, the final axial propagation constant k_z is obtained. Some experimental and theoretical results obtained by equivalent procedures were presented in Ref. 13. All of the propagation constants and field decay coefficients in Chapter 3 were obtained by this generalized effective dielectric constant method.

B. Appendix B: Determination of Scattering Coefficients

Consider again the distributed directional coupler of Figure 14. If port 1 is excited, the energy is coupled to port 3. From the directional properties of the dielectric coupler, and with the assumption that there is no reflection at either end of the coupler, no energy is coupled to port 4. With port 1 excited by an electric field of normalized amplitude $E_1 = 1$, we have

$$E_I(0) = 1/0 \quad (B-1)$$

$$E_{II}(0) = 0 \quad (B-2)$$

and for $0 < z < \ell$

$$E_I(z) = E_e e^{-jk_{\text{even}} z} + E_o e^{-jk_{\text{odd}} z} \quad (B-3)$$

$$E_{II}(z) = E_e e^{-jk_{\text{even}} z} - E_o e^{-jk_{\text{odd}} z} \quad (B-4)$$

where $E_I(z)$ and $E_{II}(z)$ are the fields along the guides I and II; E_e and E_o are the amplitudes of the fields of the even and odd modes of the coupled structure; and k_{even} and k_{odd} are the propagation constants of the even and odd modes, respectively.

Since the coupler is symmetric about the z -axis, the even and odd modes will carry equal amounts of energy. Letting $E_e = E_o$ and $z = \ell$, Equations (B-3) and B-4) become

$$E_I(\ell) = t = \frac{1}{2} (e^{-jk_{\text{even}} \ell} + e^{-jk_{\text{odd}} \ell}) \quad (B-5)$$

$$E_{II}(\ell) = c = \frac{1}{2} (e^{-jk_{\text{even}} \ell} - e^{-jk_{\text{odd}} \ell}) \quad (B-6)$$

where t and c are the transmission coefficients relating port 1 to 2, and port 1 to 3, respectively.

These equations can be rearranged as follows:

$$t = e^{-j\left(\frac{k_{\text{even}} - k_{\text{odd}}}{2}\right)l} \cos\left(\frac{k_{\text{even}} - k_{\text{odd}}}{2}l\right) \quad (\text{B-7})$$

and

$$c = -je^{-j\left(\frac{k_{\text{even}} - k_{\text{odd}}}{2}\right)l} \sin\left(\frac{k_{\text{even}} - k_{\text{odd}}}{2}l\right) \quad (\text{B-8})$$

The scattering coefficients are defined as

$$|S_{21}| = |t| = \left| \cos\left(\frac{k_{\text{even}} - k_{\text{odd}}}{2}l\right) \right| \quad (\text{B-9})$$

$$|S_{31}| = |c| = \left| \sin\left(\frac{k_{\text{even}} - k_{\text{odd}}}{2}l\right) \right| \quad (\text{B-10})$$

where, by conservation of energy, $|S_{21}|$ and $|S_{31}|$ satisfy

$$|S_{21}|^2 + |S_{31}|^2 = 1. \quad (\text{B-11})$$

VI. LISTS OF REFERENCES

- [1] S. E. Miller, "Coupled wave theory and waveguide applications," Bell Syst. Tech. J., vol. 33, no. 3, pp. 661-719, May 1954.
- [2] E. A. Marcatili, "Dielectric rectangular waveguide and directional coupler for integrated optics," Bell Syst. Tech. J., vol. 48, no. 7, pp. 2071-2102, 1969.
- [3] D. Marcuse, "The coupling of degenerate modes in two parallel dielectric waveguides," Bell Syst. Tech. J., vol. 50, no. 6, pp. 1791-1816, 1971.
- [4] T. Itanami and S. Shindo, "Channel dropping filter for millimeter-wave integrated circuits," IEEE Trans. Microwave Theory Tech., vol. MTT-26, no. 10, pp. 759-769, Oct. 1978.
- [5] I. Anderson, "On the coupling of degenerate modes on nonparallel dielectric waveguides," IEEE J. Microwaves Opt. and Acoust., vol. 3, no. 2, pp. 56-58, Mar. 1979.
- [6] K. Solbach, "The calculation and the measurement of the coupling properties of dielectric image lines of rectangular cross section," IEEE Trans. Microwave Theory Tech., vol. MTT-27, no. 1, pp. 54-58, Jan. 1979.
- [7] P. P. Toullos and R. M. Knox, "Rectangular dielectric image lines for millimeter wave integrated circuits," Western Electronics Show and Convention, Los Angeles, California, Aug. 1970.
- [8] M. J. Aylward and N. Williams, "Feasibility study of insular guide millimeter wave integrated circuits," AGARD conference on millimeter and submillimeter-wave propagation and circuits, Munich, W. Germany, Reprint no. 245, pp. 30-1 to 30-11, Sept. 4, 5, 1978.
- [9] T. N. Trinh and R. Mittra, "Coupling characteristics of dielectric waveguide of Rectangular cross-section," 1980 IEEE MTT-S International Microwave Symposium, pp. 214-217, May 1980.
- [10] W. Schlosser and H. G. Unger, "Partially filled waveguides and surface waveguides of rectangular cross section," Advances of Microwaves, vol. 1, New York: Academic Press, pp. 319-387, 1966.
- [11] J. E. Goell, "A circular-harmonic computer analysis of rectangular dielectric waveguides," Bell Syst. Tech. J., vol. 48, no. 7, pp. 2133-2160, Sept. 1969.
- [12] R. M. Knox and P. P. Toullos, "Integrated circuits for the millimeter through optical frequency range," in Proc. Symp. Submillimeter waves, Polytechnic Press of Polytechnic Institute of Brooklyn, Brooklyn, NY, 1970, pp. 497-516.

- [13] P. Yang, "A new method for the analysis of dielectric waveguides for millimeter wave and optical integrated circuits," Coordinated Science Laboratory Report R-813, University of Illinois at Urbana-Champaign, May 1978.
- [14] R. Mendez, R. Mittra, P. Yang and N. Deo, "Effective graded-index guides for millimeter-wave applications," IEEE J. Microwaves Opt. and Acoust., vol. 3, no. 2, pp. 56-58, Mar. 1979.

DATE
FILME